Bioinformatic discovery of type 11 secretion system (T11SS) cargo across the Proteobacteria

Authors: Alex S. Grossman[1,2], Nicholas C. Mucci[1], Sarah J. Kauffman[1], Jahirul Rafi[1], Heidi Goodrich-Blair[1,*]

[1]Department of Microbiology, University of Tennessee, Knoxville, Knoxville, TN 37996-0845

[2]Current address: The ADA Forsyth Institute, 100 Chestnut St, Somerville, MA 02143

[*]To whom correspondence should be addressed: hgblair@utk.edu

Keywords: Co-occurrence; T11SS, Host-association; Cargo detection; Plasmin-sensitive protein; DUF1194.

Graphical abstract:

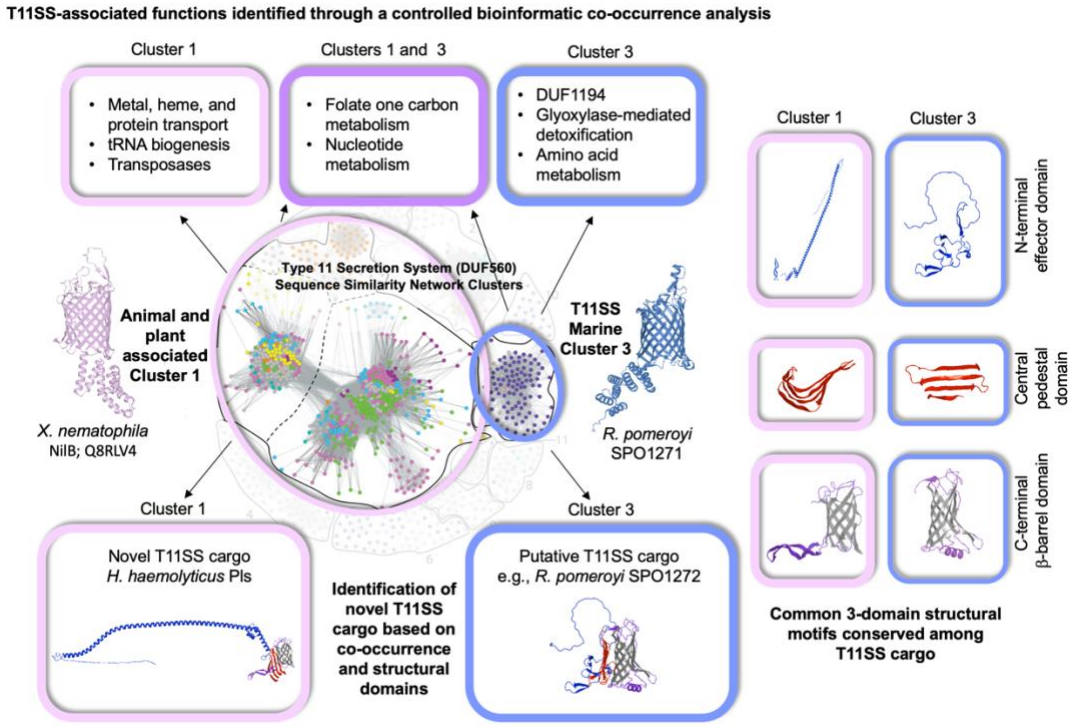
T11SS-associated functions identified through a controlled bioinformatic co-occurrence analysis
Cluster 1
Metal, heme, and protein transport
tRNA biogenesis
Transposases
Clusters 1 and 3
Folate one carbon metabolism
Nucleotide metabolism
Cluster 3
DUF1194
Glyoxylase-mediated detoxification
Amino acid metabolism
Type 11 Secretion System (DUF560) Sequence Similarity Network Clusters
Animal and plant associated Cluster 1
X. nematophila
NilB; Q8RLV4
T11SS Marine Cluster 3
R. pomeroyi
SPO1271
Cluster 1
Novel T11SS cargo
H. haemolyticus Pls
Identification of novel T11SS cargo based on co-occurrence and structural domains
Cluster 3
Putative T11SS cargo
e.g., R. pomeroyi SPO1272
Cluster 1
Cluster 3
N-terminal effector domain
Central pedestal domain
C-terminal β-barrel domain
Common 3-domain structural motifs conserved among T11SS cargo

13

Abstract:

Type 11 secretion systems (T11SS) are broadly distributed among proteobacteria, with more than 3000 T11SS family outer membrane proteins (OMPs) comprising 10 major sequence similarity network (SSN) clusters. Of these, only 7, all from animal-associated cluster 1, have been experimentally verified as secretins of cargo, including adhesins, hemophores, and metal binding proteins. To identify novel cargo of a more diverse set of T11SS, we identified gene families co-occurring in gene neighborhoods with either cluster 1 or marine microbe-associated cluster 3 T11SS OMP genes. We developed bioinformatic controls to ensure perceived co-occurrences are specific to T11SS, and not general to OMPs. We found that both cluster 1 and cluster 3 T11SS OMPs frequently co-occur with single carbon metabolism and nucleotide synthesis pathways, but that only cluster 1 T11SS OMPs had significant co-occurrence with metal and heme pathways, as well as with mobile genetic islands, potentially indicating diversified function of this cluster. Cluster 1 T11SS co-occurrences included 2556 predicted cargo proteins, unified by the presence of a C-terminal β-barrel domain, which fall into 141 predicted UniRef50 clusters and approximately 10 different architectures: 4 similar to known cargo and 6 uncharacterized types. We experimentally demonstrate T11SS-dependent secretion of an uncharacterized cargo type with homology to Plasmin sensitive protein (Pls). Unexpectedly, genes encoding marine cluster 3 T11SS OMPs only rarely co-occurred with the C-terminal β-barrel domain and instead frequently co-occurred with DUF1194-containing genes. Overall, our results show that with sufficiently large-scale and controlled genomic data, T11SS-dependent cargo proteins can be accurately predicted.

35 **Impact Statement:** We describe a novel method for controlling genomic neighborhood analyses
36 and use this controlled co-occurrence technique to examine two distinct clusters of genes from
37 the recently described type 11 secretion system (T11SS): Cluster 1, predominantly encoded by
38 host-associated microbes and Cluster 3, encoded by marine microbes. We found that both
39 clusters of predicted T11SS frequently co-occur with single carbon metabolism and nucleotide
40 synthesis pathways, but only the host-associated cluster co-occurred with iron uptake
41 pathways. Using these datasets, we predicted 2687 T11SS dependent cargo with approximately
42 ten unique architectures, six of which have not previously been linked to T11SS. Finally, we
43 validate our results by demonstrating T11SS-dependent secretion of a cargo protein with one of
44 the novel architectures, plasmin-sensitive surface protein Pls from *Haemophilus*
45 *parahaemolyticus*.

46 **Data Summary**

47 This paper describes genomic co-occurrences of T11SS OMP sequences originally identified
48 through sequence similarity networking in a previous publication [3] as constituents of
49 similarity clusters, 1 and 3. Accession IDs and assorted metadata for those clusters/networks
50 are listed in Table S1 of that article: https://journals.asm.org/doi/suppl/10.1128/mbio.01956-
51 21/suppl_file/mbio.01956-21-st001.xlsx. All other supporting data, accession IDs, code, and
52 protocols have been provided within this article or through supplementary data files.
53 Additionally, all supplemental data are available on Figshare
54 (https://doi.org/10.6084/m9.figshare.28514069.v2) [1].

55 **Introduction**

56 Identifying protein function remains a difficult task in the postgenomic age. As of
57 12/02/2024 there were 5,366 domains of unknown function (DUF) families, which constitutes
58 around 22.6% of the database [2]. This means roughly one quarter of the Pfam database
59 remains uninvestigated, limiting our understanding of the breadth of biological processes
60 occurring on Earth. Functional characterization of proteins with DUF domains enables their
61 annotation and removal from the DUF list, improving our datasets permanently. *In silico*
62 approaches applied to protein domains are an important component of this process, as they
63 can focus attention on the likely functions of a particular protein family [3]. Recently, a
64 combination of *in silico* and experimental approaches has yielded insight into the DUF560
65 protein family of outer membrane proteins (OMPs), defining it as the type 11 bacterial
66 secretion system (T11SS), represented by 10 distinct sequence-level clusters [4]. T11SS are
67 outer membrane proteins that translocate either soluble proteins or membrane anchored
68 lipoproteins from the periplasmic space to the extracellular space [4]. Presumably cargo
69 proteins are transported in an unfolded state, since some cargo are dependent on Skp
70 chaperones [5]. T11SS homologs are present among a diverse array of Proteobacteria, including
71 human pathogens in the *Neisseria*, *Haemophilus*, and *Moraxella* genera [6–8]. In the gamma-
72 proteobacterium *Xenorhabdus nematophila*, a T11SS system encoded within the nematode
73 intestinal localization locus (*nil*) is necessary for colonization of the mutualistic nematode host
74 *Steinernema carpocapsae* [9]. In this system the T11SS, NilB, regulates the surface exposure of a
75 surface lipoprotein, NilC, both of which are necessary for colonization. Other known lipidated
76 T11SS-dependent cargo include well studied pathogenesis factors such as the metal uptake co-
77 receptors transferrin binding protein B (TbpB) and lactoferrin binding protein B (LbpB), as well

78 as factor H binding protein, which binds an immune activation factor [6–8, 10, 11]. These cargo
79 are composed of two types of domains, variable N-terminal effector domains and 8-stranded C-
80 terminal β-barrel domains (such as TbpBBD and Lipoprotein C). T11SS can transport
81 unlipidated, soluble cargo proteins across the outer membrane. For example, T11SS-dependent
82 hemophilin homologs have been characterized from *X. nematophila* (HrpC), *Acinetobacter*
83 *baumannii* (HphA), and *Haemophilus haemolyticus* (Hpl) [4, 10, 12, 13]. However, the majority
84 of T11SS OMPs do not have a known or predicted cognate cargo. A sequence similarity network
85 analysis suggested that experimentally characterized T11SS only capture a small portion of the
86 functional diversity present in this family [4].

87 The availability and accessibility of sequencing data have skyrocketed since the first
88 bacterial genome was sequenced in 1995, with ~315,000 prokaryotic genomes on RefSeq [14].
89 This tremendous repository of genomic sequence data allows computational biologists to probe
90 these genomes for patterns in genetic co-occurrence, as measured through proximity to a gene
91 of interest. Genes within a common functional pathway often cluster together within a
92 genome. Such patterns can be useful when forming hypotheses about the function of
93 uncharacterized proteins. Gene neighborhood studies analyze the genomic regions upstream
94 and downstream of any given gene of interest with the assumption that nearby genetic
95 partners could illuminate the role(s) of the unknown gene [15].

96 However, one flaw in the current methodology used to derive co-occurrence lists is the
97 lack of bioinformatic controls capable of removing non-specific co-occurring genes. For
98 example, commonly inherited, deeply ancestral domains, such as transcription and translation
99 machinery, often appear as the top result of a co-occurrence analysis, but do not yield useful

100 information about the specific query gene since their appearance is a coincidence of ubiquity
101 [16]. Also, meaningful results can be obscured by co-occurrence based on structural or other
102 common features present within the query protein, such as those that target the gene product
103 to specific cellular locations, which are expected to interact commonly with the relevant
104 protein trafficking machinery. Herein, we use computational approaches to elucidate potential
105 functional roles played by T11SS-dependent cargo and predict novel cargo. Using these results,
106 we then generated a co-expression system in *Escherichia coli* to experimentally demonstrate
107 the secretion of one novel, bioinformatically predicted cargo family using the plasmin sensitive
108 protein (Pls) from *Haemophilus parahaemolyticus* and the type eleven Pls Secretor (TepS).

109 **Methods**

110 **Gene neighborhood analysis**

111 The T11SS genome neighborhoods (±6 genes around a T11SS gene) from cluster 1 (1111
112 queries) and cluster 3 (145 queries) [4] were analyzed. T11SS genome neighborhoods were
113 generated through Rapid ORF Detection & Evaluation Online (RODEO) [17]. As described in the
114 main text, a control was developed to identify and remove non-specific genes from among
115 those flagged as co-inherited or syntenic with T11SS (Fig. 1). The primary control list was
116 generated by extracting all GO-term outer membrane proteins from proteobacteria and
117 filtering for sequences similar in length to the median T11SS length (480 – 482 amino acids in
118 length) and removing all DUF560-containing proteins. For both T11SS cluster analyses a random
119 subset of control sequences were chosen equal to the number of queries being analyzed.
120 Controlled protein sequences were downloaded from UniProt [18] in February 2021. Co-

121 occurring protein domains were annotated and summed up to determine frequency among
122 queries and controls. False Discovery Rate was calculated by dividing frequency among T11SS
123 queries and control sequences. All domains with and FDR > 0.1 were excluded from analysis.
124 For cluster 1 all domains with fewer than 25 occurrences were excluded. For cluster 3 all
125 domains with fewer than 5 co-occurrences were excluded.

126 The Joint Genome Institute Integrated Microbial Genomes and Microbiomes platform
127 (https://img.jgi.doe.gov/) [19, 20] was used to examine genomic regions surrounding the T11SS
128 OMPs-encoding genes of select cluster 3 bacteria. Briefly, the "find genes" function was used to
129 identify T11SS OMP homologs from selected representatives of the Roseobacteriaceae and
130 Rhodobacteraceae. The "gene neighborhoods" function was then used to visualize the regions
131 surrounding the T11SS OMP homologs and to identify syntenic loci (for an example, see
132 Supplemental File 3, Neighborhood Alignment Tab). Predicted structures were downloaded as
133 .pdb or .cif files from AlphaFold 2.0 [21, 22] except in one instance (*Amylibacter cionae* CGMCC
134 1.15880 IEX10_RS12250) for which an AlphaFold 3.0 model [23] was used to predict the
135 structure, and a .pdb file of the top ranked prediction was used for Fig. 8G [21]. Average
136 predicted local distance difference test (pLDDT) values for each predicted structure are
137 provided in Supplementary File 1 (Tab AlphaFold Predicted Structures) Using each .pdb file,
138 structural motifs were highlighted using Protean 3D®, Version 17.4.3, DNASTAR, Madison, WI.

139

140 **Functional and structural analyses of co-occurring gene neighborhood domains**

141 Protein sequences that contain domains that co-occur with T11SS from the gene
142 neighborhood analysis (Supplemental file 1, Cluster1FDR_Threshold tab) were obtained via
143 UniProt [18]. KofamKOALA [24] and BlastKOALA [25] were used to assess function.
144 KofamKOALA assigns KEGG orthology to user sequence data by HMMER/HMMSEARCH against
145 the KEGG database. BlastKOALA is similar but uses a BLAST search to assign KEGG orthology.
146 Genes were matched to BRITE hierarchies to assess general cellular function and KEGG pathway
147 to assess potential interactions.

148 To identify potential cargo proteins all downloaded protein sequences were matched to
149 UniRef50 clusters to compress potential homologs [26]. The reference sequences from these
150 UniRef50 clusters where then subjected to a BLAST search against known T11SS cargo β-barrel
151 and handle domains (nematode intestine localization protein (NilC) in *Xenorhabdus*
152 *nematophila*, transferrin binding protein (TbpB) N-terminal and C-terminal in *Xenorhabdus*
153 *nematophila*, heme receptor protein (HrpC) in *Xenorhabdus nematophila*, Cobalt receptor
154 protein (CrpC) in *Xenorhabdus cabanillasii*, Hemophilin (Hpl) in *Haemophilus haemolyticus*,
155 hemophilin (HphA) in *Acinetobacter baumanii*, factor H binding protein (fHbp) *Neisseria*
156 *meningitidis*, and lactoferrin binding protein (LbpB) N-terminal and C-terminal in *Neisseria*
157 *meningitidis* to search for homologs of T11SS cargo with a low stringency E-value filter of <0.05
158 in order to find even distantly related homologs, generating a list of 141 potential cargo
159 proteins from cluster 1 and a single potential cargo from cluster 3. MSA alignment was used to
160 group the predicted cargo proteins into distinct architectures. 10 groups emerged, TbpB-like,
161 LbpB-like, Hemophilin-like 1 and 2, fHbp-like, Pls-like, highly disordered N-terminus 1 and 2,
162 *Psychrobacter* surface protein, and *Sphingomonas* surface protein. Structural data predictions

163 for the 9 architectures which contained more than one sequence were generated through
164 PSIPRED [27] for secondary structure and AlphaFold2 [21, 22] for tertiary structure.

165

166 **Co-expression of Pls and its cognate T11SS protein TepS**

167 All cultures were grown in glucose minimal media supplemented with 1% LB. Plate
168 based cultures were grown on glucose minimal plates [28]. For plasmid-based expression,
169 chemically competent *Escherichia coli* strain BL21-DE3 (C43) were chosen for ease of
170 transformation and their ability to non-toxically express membrane proteins [29, 30]. Strains of
171 *E coli* were grown at 37°C. Where appropriate media was supplemented with ampicillin at a
172 concentration of 150 µg/ml. Protein expression was induced at the midlog point of bacterial
173 growth via addition of isopropyl β-d-1-thiogalactopyranoside (henceforth IPTG) at a
174 concentration of 0.5mM.

175 Using sequences from *H. parahaemolyticus* strain NCTC10794, GenScript synthesized
176 genes for Plasmin sensitive surface protein (Pls-STO63610.1) with an attached C-terminal FLAG
177 tag and its genomically associated T11SS OMP (TepS-STO63613.1) with an N-terminal 6xHis tag.
178 Both genes were codon optimized for expression in *E. coli* Bl21DE3. GenScript cloned Pls-FLAG
179 into multiple cloning site 1 of pETDuet-1 and 6xHis-TepS into multiple cloning site 2, resulting in
180 expression plasmids pETDuet-1/Pls-FLAG and pETDuet-1/Pls-FLAG/6xHis-TepS. Expression
181 plasmids were transformed into *E. coli* via electroporation. Strains were grown in defined
182 medium with 150 mg/ml ampicillin [31]. Bacteria were subcultured into 100 ml of broth at an

183 initial optical density at 600 nm (OD_{600}) of 0.1, grown for 6 h at 37°C to reach late logarithmic
184 growth, and induced with 0.5 mM IPTG for 1 hour.

185 **Pls detection assays**

186 Two approaches were taken to monitor localization of Pls: immunoblotting (dot blot and
187 Western) and immunofluorescence and flow cytometry. For the immuno-dot blot, cells were
188 normalized to an OD600 of 1, rinsed 3x, lysed by sonication for 30 sec at ~500 root mean square
189 volts (V_{rms}), and spotted in technical triplicate on nitrocellulose membranes to enumerate total
190 cellular Pls. To monitor extracellular secretion of Pls supernatant was collected from cultures
191 after induction and filtered sterilized to remove all cells. Supernatant samples were
192 ultracentrifuged at 150,000 relative centrifugal force (RCF) for 3 h to separate the soluble
193 fraction from the insoluble component, composed of cell membrane components and
194 membrane vesicles. Previous studies have detected both T11SS OMPs and cargo within
195 membrane vesicles, necessitating their removal from supernatants [4, 32]. The membrane
196 vesicle fraction was suspended in protein sample buffer. 700 µl of each soluble supernatant
197 fraction was precipitated via 10% trichloroacetic acid (TCA) and the resulting pellet was
198 suspended in protein sample buffer [33]. Samples were analyzed by 10% sodium dodecyl
199 sulfate-polyacrylamide gel electrophoresis (SDS-PAGE) and immunoblotting. All dot blots and
200 Western blots were probed with rat anti-FLAG primary antibody and goat anti-rat secondary
201 antibody conjugated to a 680nm fluorophore. Intensities were recorded for FLAG reactive
202 bands. For every supernatant sample, a band from the Coomassie blue-stained gel was used as
203 a loading control to normalize intensities of supernatant samples prior to analysis. Fold change
204 of secretion was determined by dividing the amount of supernatant Pls detected in the

205 Pls/TepS co-expression treatment by the amount detected in the Pls alone treatment. A Tukey's
206 honestly significant difference (HSD) test was used for comparing fold change of secretion [34].

207 For immunofluorescence labeling and detection of Pls, overnight cultures of strains
208 were washed thrice with PBS, and resuspended in defined medium at an OD_{600} of 0.05. Cultures
209 were then grown to mid-log phase and one replicate culture of every strain was induced with
210 IPTG at a final concentration of 0.5 mM, while the other culture was left uninduced. All strains
211 were allowed to grow for an additional 1.5 h at 30°C with shaking. Cells were blocked from
212 nonspecific binding using 3% BSA in PBS and incubated with a 1:300 dilution of DYKDDDDK Tag
213 Recombinant Rabbit Monoclonal Antibody Alexa Fluor Plus 488 (Invitrogen) in 0.5% BSA in PBS.
214 Cells were washed thrice in 0.5% BSA in PBS, fixed with 4% formaldehyde in PBS for 15 min, and
215 washed thrice with PBS. Cells were resuspended in PBS and then passaged through a Cytoflex
216 (Cytek NL-3000) and 100,000 events were captured. Visualization and data analyses were
217 performed in FlowJo (Beckton, Dickinson and Company, Franklin Lakes, NJ, USA). Flow
218 cytometry analysis was performed three separate times, and for each experiment three
219 biological replicates were performed, resulting in a total of 9 biological replicates. To monitor
220 total Pls levels expressed, samples from cultures grown for flow experiment were pelleted,
221 washed with PBS, and frozen at -20 for 24 h before being resuspended in PBS and lysed by
222 sonication for 1 min total (5s on, 10s off, 600 V_{rms}). After pelleting cellular debris, the protein
223 concentrations of the cell lysate supernatants were determined using the Pierce 660nm Protein
224 Assay Reagent. All samples were normalized and 9 µg of total protein for each treatment were
225 separated by SDS-PAGE gel, followed by Western blot probing with primary anti-DYKDDDDK

226 antibody (63703 Biolegend) at a 1:10,000 dilution and secondary IRDye 680RD Goat anti-Mouse
227 (926-68070) at a 1:10,000 dilution. Blots were imaged using an Odyssey FC.

228

229 **Results:**

230 **Establishing a control for domain of unknown function (DUF) gene neighborhood co-**
231 **occurrence analysis**

232 Characterized T11SS-cargo pairs encoded by Proteobacteria typically have conserved
233 roles in host-metal acquisition and immune evasion [4, 8, 10, 12]. Only a small portion of
234 predicted T11SS-cargo pairs has been experimentally characterized, leaving open the possibility
235 that as-yet uncharacterized systems may be participating in diverse symbiotic and metabolic
236 pathways. To gain insights into the potential breadth of biological processes in which T11SS-
237 cargo pairs may function, we collected all T11SS sequences identified as part of the largest
238 T11SS sequence similarity network cluster described in Grossman et al., 2021 (cluster 1,
239 containing 1111 genes) and utilized the Rapid ORF Description & Evaluation Online (RODEO)
240 software to identify all protein domains encoded within their T11SS loci, herein defined as six
241 open reading frames upstream or downstream of the T11SS OMP query genes. Analysis of all
242 loci resulted in a data set of 1504 domains, co-occurring between 2 and 928 times
243 (Supplemental file 1, Cluster1Co tab) [17]. To avoid spurious correlations, we chose to exclude
244 any domains that co-occurred fewer than 25 times (~2.7% of the maximum frequency co-
245 occurrence). This number was arrived at by generating a histogram of co-occurrence frequency
246 and identifying the inflection point between the rare co-occurring sequences which made up

247 the bulk of the dataset (1331 or 88.5%) and those domains whose co-occurrence frequency was
248 greater than expected randomly (173 or 11.5%) (Fig. S1).

249 To ensure that the observed co-occurrences were specific to the T11SS protein family
250 and not due to common features of genomic loci encoding outer membrane proteins, we
251 developed and implemented a control process. Briefly, RODEO co-occurrence neighborhoods
252 were generated using randomly selected proteins with biophysical characteristics similar to our
253 DUF560 query proteins such as protein length and outer membrane localization (GO term:
254 outer membrane GO0019867), and then used as a point of comparison for gene neighborhoods
255 from T11SS genes. The control sequences obtained were limited to the Proteobacteria phylum,
256 where T11SS predominantly occur [4]. Due to a left-skewed distribution, the median length of
257 all DUF560 domain containing proteins in Pfam (accessed February 2021) was used to reduce
258 bias from pseudogenes and gene fragments (Fig. S2) [2]. The median size of all predicted T11SS
259 proteins was 481 amino acids, so we extracted all outer membrane ORFs between 480 and 482
260 amino acids in size. Sequences that appeared in the T11SS database were removed from the
261 control database to ensure unbiased selection. A random subsample of this control database
262 was taken equal to the number of sequences in the original query database (Supplemental file
263 1, ControlQueries tab) (Fig. 1).

264 OMP sequences from the subsampled control dataset were then submitted as a query
265 to the genome neighborhood network function of RODEO using the same parameters as the
266 T11SS query list. The output of this control co-occurrence analysis was used to generate a false
267 discovery rate (FDR) for any given domain by dividing frequency of co-occurrence with random
268 OMPs by frequency of co-occurrences with T11SS genes. We then gated the dataset for

269 domains with an FDR less than 0.1 (10%) to exclude non-specific correlations, resulting in a final
270 set of 51 significantly co-occurring domains. (Supplemental file 1, Cluster1FDR_Threshold tab).
271 The most common significant co-occurring domains alongside cluster 1 T11SS OMPs were other
272 DUF560 proteins (928/1111), the TbpBBD β barrel domain (503/1111), the TonB C-terminal
273 domains (364/1111), heme oxygenase (137/1111), and DUF454 (118/1111). Next, all genes that
274 co-occurred with a cluster 1 T11SS gene and possessed one of the identified domains were
275 extracted resulting in 3405 significantly co-occurring genes (Supplemental file 1,
276 Cluster1SigGenes tab). These genes were submitted to KofamKOALA and BlastKOALA in parallel
277 for annotation into molecular pathways and BRITE hierarchies [24, 25].

278

279 **Functional assessment of T11SS co-occurring proteins identifies a role of iron uptake, protein**
280 **export, and single carbon metabolism**

281 We examined the co-occurrence gene set for those with annotations in the curated
282 Kyoto Encyclopedia of Genes and Genomes (KEGG) ortholog (KO) database [24, 35]. A hidden
283 Markov model search using KofamKOALA (HMMER/HMMSEARCH) was used to annotate the
284 genes according to the KO database. The software found matches for 1488 of the 3405
285 significant co-occurring genes (Supplemental file 2, Cluster1KofamBrite tab). When matched to
286 cellular functions (BRITE hierarchies) the most common categories were transporters
287 (periplasmic TonB, ExbD, Signal peptidase II, TolA, etc.), enzymes (heme oxygenase, formate
288 dehydrogenase, exopolyphosphatase, dihydrofolate reductase, etc.), and tRNA biogenesis
289 (tRNA modifying GTPase, tryptophanyl-tRNA synthase, Ribonuclease P, aminoacyl tRNA

290 synthase) (Fig. 2A). Additionally, cluster 1 T11SS genes were found to significantly co-occur with
291 transposase genes. Of the 1488 matched sequences, 259 had known pathway association, most
292 commonly biosynthesis of secondary metabolites (heme oxygenase, cobalamin-dependent
293 methionine synthase, vitamin K biosynthesis protein MenH, etc.), porphyrin metabolism (heme
294 oxygenase), and protein export (signal peptidase II and YidC insertase) (Fig. 2B) (Supplemental
295 file 2, Cluster1KofamPath tab). The list of pathways also included aminoacyl tRNA biosynthesis
296 (TyrS, TrpS). A high frequency of co-occurrence with transposases and tRNA synthesis genes is
297 characteristic of pathogenicity islands, phage regions, and other mobile genetic elements, since
298 many mobile genetic elements have targeted insertion sites near universally conserved
299 features, such as tRNA genes [36]. Co-occurrence with mobile genetic island signifiers supports
300 our previous observation of horizontal acquisition of a T11SS in *X. nematophila* [4, 9].. Finally,
301 the list included several carbohydrate biosynthesis pathways (hsa00670, one carbon pool by
302 folate; map00230, purine metabolism).

303 To further functionally annotate co-occurrences, we used BLAST alignment, rather than
304 hidden Markov searching, to establish sequence similarity using BlastKOALA, which compares
305 query sequences to the non-redundant KEGG dataset [25]. The software found matches for
306 1387 of the 3405 significantly co-occurring genes. Categorization into cellular functions (BRITE
307 hierarchies) again revealed the largest categories to be enzymes, transporters, and tRNA
308 biogenesis (Fig. S3A) (Supplemental file 2, Cluster1BlastBrite tab). BlastKOALA identified more
309 co-occurring amino acid importers (arginine, lysine, tyrosine, tryptophan, and serine
310 transporters) in the dataset than KofamKOALA. Of the 1387 identified genes, 260 had known
311 pathways. This analysis identified similar pathways to those identified by KofamKOALA,

312 including secondary metabolite biosynthesis, protein export, porphyrin metabolism, and
313 carbohydrate biosynthesis (Fig. S3B) (Supplemental file 2, Cluster1BlastPath tab).

314

315 **Predicted structure analysis of putative cluster 1 T11SS cargo reveals variable N-termini and**
316 **shared C-terminal domains**

317 To bioinformatically identify potential cluster 1 T11SS-dependent cargo we searched co-
318 occurring protein sequences for homology to domains of experimentally demonstrated cargo
319 (NilC, TbpB, LbpB, fHbp, HrpC, CrpC, Hpl, and HphA) [4, 7, 12]. The 3405 sequences significantly
320 co-occurring with cluster 1 were first consolidated using UniProt ID mapper into 666 UniRef50
321 clusters with 50% or greater identity at an amino acid level (Supplemental file 1, Cluster1Uniref
322 tab) [26]. The reference sequences of these UniRef50 were next searched using BLASTp for
323 sequence similarity with N-terminal domains and C-terminal β-barrel domains from
324 experimentally verified T11SS cargo proteins: NilC, TbpB, LbpB, HrpC, CrpC, Hpl, and Factor H
325 binding protein, with a low stringency E-value cutoff of 0.05 [4, 7, 8]. No matches were found
326 for NilC or the N-terminal ligand binding domain of fHbp, but all other queries matched at least
327 one cluster. This analysis revealed 141 clusters of potential T11SS-dependent cargo proteins
328 representing 2656 ORFs across 1048 species/taxa (Supplemental file 1, Cluster1PutativeCargo
329 tab). Each sequence was also annotated with SignalP 6 [37, 38] which predicted 81 Sec secreted
330 lipoproteins, 33 Sec secreted soluble proteins, and 27 proteins with no predicted signal peptide
331 (3 of which were annotated as fragments). For our purposes, we defined a lipoprotein as any
332 predicted to be membrane anchored via tri-acylation of a C-terminal cysteine. Soluble proteins

333 were defined as those predicted to have a Sec (or Tat) signal peptide and that lacked predicted
334 transmembrane features. Overall, the fact that the majority of identified T11SS cargo
335 candidates are predicted to have a signal peptide is consistent with published evidence that
336 T11SS transport Sec dependent lipoproteins and soluble proteins [4, 7].

337 We utilized multiple sequence alignment to separate the predicted cargo protein
338 clusters into distinct, annotated architectures (secondary structures in Fig 3, tertiary structures
339 in Fig 4, Supplemental file 1, Cluster1PutativeCargo tab). This analysis identified two distinctive
340 groups of Hemophilin-like proteins based on homology to known hemophilins (Hpl, HrpC,
341 HsmA), the predominantly soluble group 1 (96 lipoproteins, 912 soluble) and the predominantly
342 lipidated group 2 (65 lipoproteins, 7 soluble), a group of TbpB-like proteins (638 lipoproteins, 7
343 soluble), a group of proteins annotated as fHbp-like proteins by virtue of their Lipoprotein C
344 domain (54 lipoproteins, 285 soluble), and a group of lactoferrin-binding protein-like proteins
345 (105 lipoproteins).

346 Several categories with no characterized representatives also emerged. Two lipoprotein
347 architectures with an elongated, disordered N-terminal region occurred: disordered N-terminus
348 1 (196 lipoproteins, 8 soluble) and 2 (1 lipoprotein only). Another group was named Pls-like
349 proteins (173 lipoproteins, 20 soluble) because of homology to the repeat rich (EEARKA motif)
350 α-helix from Pls surface glycoproteins in *Staphylococcus aureus* . Two phylogenetically-
351 restricted architectures were observed with multiple TbpBBD domains, *Sphingomonas* surface
352 proteins, which have an N-terminal sequence of proline-threonine repeats (18 lipoproteins, 12
353 soluble) and *Psychrobacter* surface proteins which have an N-terminal sequence of ~12 proline-
354 threonine-aspartic acid repeats (PTD motif) (55 lipoproteins, 4 soluble). Proline-threonine

355 repeats occur in *Xanthomonas campestris* endoglucanase, where they provide elasticity and
356 facilitate enzyme positioning around its substrate [39]. The PTD motif is found in a family of
357 *Gracilibacteria* (BD1-5) surface proteins and in the eukaryotic microbe *Plasmodium falciparum*
358 and are hypothesized to act as adhesins facilitating interactions with hosts [40, 41].

359 Using PsiPred 4.0 [27] and AlphaFold2 [21] we predicted the secondary and tertiary
360 structures of representative proteins from the largest UniRef50 cluster from each architecture
361 with more than one representative (Fig. 3 and Fig. 4). All of the architectures were predicted to
362 have at least one domain, generally at the C-terminus, composed of β-strands linked by
363 disordered loops that form a C-terminal β-barrel domain similar to the TbpBBD domain or the
364 Lipoprotein C domain. The N-terminal domains of most cargo had β-strands predicted to form
365 handle domains like those seen in hemophilin or TbpB [4, 7]. When present, the disordered
366 regions and long α-helical repeat regions preceded this handle domain.

367 When examining secondary and tertiary structures in parallel we noticed that the
368 predicted cargo form three distinctive structural regions: a common C-terminal 8-stranded β-
369 barrel domain, a common central region formed by β-strands, which we have termed a
370 "pedestal" region based on its positioning as a platform for a variable N-terminal domain
371 "effector" domain, predicted to serve the functional role specific to each cargo protein type.
372 Using solved crystal structures where available [6, 10, 42], and Alphafold2 or Alphafold3 models
373 for representative cargo proteins [21], we divided the predicted cargo structures into these
374 three regions and categorized them by recurrent patterns (Fig. 5). The predicted central
375 pedestal-domains fell into six visibly distinguishable categories; ; 4-stranded groove (Fig. 5A),
376 wing (Fig. 5B-D), and sheet (Fig. 5E, F), 5-stranded sheet (Fig. 5G-I, and 6-stranded/extended

377 sheets (Fig. 5J, K). None of the examined pedestal regions featured complex, variable loops,
378 suggesting they may play a structural role. In contrast, the C-terminal 8-stranded β-barrel core
379 structures are embellished within each protein by diverse inter-strand loops including
380 disordered regions, extended β-strands, and α-helices that could be playing functional roles, as
381 do the loops of the N-lobe TbpBBD domain of TbpB [43].

382 The N-terminal effector domains displayed a variety of structural motifs including
383 disordered loops (Fig. 5 B-D,H, I), α-helices (Fig. 5A, E, K), β-strands (Fig. 5D,F,J), and β-barrels
384 (Fig. 5G). The examined effector regions ranged in size, with some barely extending beyond the
385 pedestal domain and others including duplications of the 8-stranded β-barrel domain. The
386 latter is typified by the solved structure of TbpB, which comprises two lobes, each containing
387 the hemophilin handle-β-barrel pair architecture (Fig. 5G). The TbpB N-lobe pair comprises the
388 effector region, while the C-lobe handle comprises the pedestal and the C-lobe barrel is the
389 putative T11SS targeting domain [42, 43]. This domain duplication and functional specialization
390 may also explain the architecture of *Sphingomonas* and *Psychrobacter* surface proteins that
391 feature 2-3 copies of the handle-barrel pair (Fig. 4). However, the long, disordered loops
392 present in those proteins likely generate a distinctive structural architecture relative to TbpB.

393

394 **Demonstrating T11SS-dependent secretion of Plasmin sensitive surface protein**

395 To assess the accuracy of our bioinformatic predictions of T11SS cargo, we
396 experimentally tested levels of secretion in *E. coli* of a representative novel cargo protein with
397 or without its predicted cognate T11SS protein. Several of our predicted cargo possess a large

398 α-helix repeat region absent from the known T11SS cargo. We chose to test a representative of
399 this group, the 525 amino acid Plasmin sensitive protein homolog (Pls) (STO63610.1) and its
400 genomically associated putative type eleven Pls secretor (TepS) (STO63613.1) from *H.*
401 *parahaemolyticus* strain NCTC10794. The *H. parahaemolyticus* Pls α-helix repeat region shares
402 between 49 and 62% identity with the repeat regions of surface glycoprotein Pls from
403 *Staphylococcus aureus* (WP_256928426, WP_256927786, WP_258808513, WP_256933640, and
404 WP_257570445) that contributes to virulence by stimulating biofilm formation [44].
405 *Staphylococcus* and *H. parahaemolyticus* Pls differ in that homologs of the former are larger
406 and lack the C-terminal β-barrel domain.

407 To experimentally test for TepS-mediated secretion of *H. parahaemolyticus* Pls, we used
408 addition of a FLAG-tag epitope to allow Pls detection and expressed this protein with or without
409 TepS using pETDuet-1 based plasmids in *E. coli* BL21 DE3 C43. Western blot analysis of lysed
410 cells revealed that Pls was effectively expressed with or without TepS co-expression, though
411 slightly more was present in/on cells expressing TepS, suggesting that surface exposure may
412 increase the amount of protein a cell can contain, or that TepS protects the protein from
413 degradation (Fig. 6A and S4AB). Flow cytometry was used to detect surface exposure of
414 membrane anchored lipoproteins. No Pls was detected on the surface of cells induced to
415 express Pls alone, however ~40% of cells had detectable surface Pls when expressing both Pls
416 and TepS (Fig. 6BC). Since Pls homologs can be cleaved spontaneously, or by proteases as in the
417 case of *S. aureus* Pls [44, 45] we used western blot immunostaining on spent culture media
418 (separated into soluble and vesicle fractions) to determine if Pls was being liberated from cell
419 surfaces (Figure 6D and S4CD). Immuno-dot-blots were performed on cell lysates after

420 collecting supernatants to ensure that comparable amounts of Pls were being produced (Fig. 6D
421 and S4E) [44, 45]Pls was present in the supernatant, but only when co-expressed with the
422 T11SS protein TepS, suggesting that *Haemophilus* Pls can be cleaved from the cell surface
423 spontaneously. [44, 45]Some Pls was located in extracellular vesicles independent of TepS
424 expression, but this amount was higher in the presence of TepS (Fig. 6 and Fig. S4). In Western
425 immunoblots, FLAG-tagged Pls is visible as a single clear band in individual replicates, but varied
426 in apparent size between biological replicates from 82.3 to 121.3 kD with an average of 103kD.
427 This is almost twice the value predicted from sequence alone (56.8kD). This large and variable
428 size may suggest that Pls is either being significantly slowed by glycan moieties as it travels
429 through polyacrylamide, its passage is being affected by its extremely high concentration of
430 charged amino acids, or that it exists as a dimer when expressed in *E. coli*.

431

432 **Bioinformatic analysis of cluster 3 T11SS proteins from marine environments reveals distinct**
433 **co-occurrence patterns**

434 To test the robustness of our analysis we then utilized our co-occurrence technique to
435 explore cluster 3 T11SS proteins, predominantly containing sequences from marine microbes.
436 Cluster 3 was chosen for in depth analysis because it is composed entirely of sequences from
437 organisms that occupy aquatic/marine environments, for which no T11SS have been described
438 in the literature and which may encode novel cargo. This cluster almost exclusively contains
439 sequences from the families *Roseobacteriaceae* and *Rhodobacteraceae* [46], including both
440 pelagic microbes and symbionts of algae (*Silicimonas algicola*) [47], mollusks (*Aliiroseovarius*

441 *crassostreae*) [48], tunicates (*Ascidiaceihabitans donghaensis*) [49], echinoderms (*Sulfitobacter*
442 *delicatus*) [50], and corals (*Roseivivax isoporae*) [51]. All genes from cluster 3 (145 sequences)
443 were used as queries in the RODEO genome neighborhood network function, using the same
444 parameters as the cluster 1 analysis, resulting in 203 co-occurring domains with frequencies
445 between 2 and 102 (Supplemental file 1, Cluster3Co tab). Domains which co-occurred fewer
446 than 5 times were excluded from analysis (122 or ~60.0%) (Fig. S1C-S1D). Co-occurring domains
447 were compared to another random subset of the non-specific control co-occurrence dataset to
448 assign FDR values. All domains with an FDR greater than 0.1 were excluded from analysis,
449 resulting in 42 significantly co-occurring domains (Supplemental file 1, Cluster3FDR_Threshold
450 tab). The most common co-occurring domains were additional DUF560/T11SS domains
451 (102/145 loci), DUF1194 (102/145 loci), glyoxalase domains (89/145 loci), and thymidylate
452 synthase/thymidylate synthase complementing protein (77/145 loci). The TbpBBD domain
453 passed the FDR threshold, however relative to the analysis of cluster 1 it was exceptionally rare
454 (8/145 loci). All genes that co-occurred with a marine cluster 3 T11SS OMP and contained any
455 of the significant co-occurring domains were extracted, resulting in 860 significant co-occurring
456 genes which we submitted to KofamKOALA and BlastKOALA for functional analysis [24, 25].

457 KofamKOALA found matches for 595 of the 860 significant co-occurring genes
458 (Supplemental file 2, Cluster3KofamBrite tab). When matched to cellular functions (BRITE
459 hierarchies) the most common categories were enzymes (lactoylglutathione lyase, thymidylate
460 synthase complementing proteins, aspartate aminotransferase, etc.), prokaryotic defense
461 systems (antitoxins CptB and HigA-1, topoisomerase IV B), and transcription factors (Cell
462 division repressor DicA, cold shock protein) (Fig. 7A). Of the 595 matched sequences, 270 had

463 known pathway association, the most common pathways being biosynthesis of one carbon pool
464 by folate (dihydrofolate reductase, thymidylate synthase), pyrimidine/nucleotide metabolism
465 (thymidylate synthase), pyruvate metabolism (lactoylglutathione lyase), and biosynthesis of
466 amino acids (aspartate aminotransferase) (Supplemental file 2, Cluster3KofamPath tab). Unlike
467 cluster 1, transposases were not among the significantly co-occurring genes of cluster 3.
468 However, aminoacyl-tRNA synthesis functions, which can be associated themselves with mobile
469 genetic elements [36, 52], do appear on the co-occurrence list, including alanyl-tRNA, prolyl-
470 tRNA, and threonyl-tRNA synthases (Fig. 7B). Parallel analysis with BlastKOALA identified 514 of
471 the 860 significant co-occurring genes, of which 267 had known pathway association
472 (Supplemental file 2, Cluster3BlastBrite and Path tabs). BlastKOALA did not identify any
473 additional cellular functions or pathways not already revealed by KofamKOALA (Fig. S5).

474

475 **Bioinformatic investigation of potential cluster 3 T11SS cargo**

476 Initial attempts to identify new cargo proteins within the co-occurrence datasets from
477 cluster 3 used the same methods used for cluster 1. UniRef50 clustering with ≥50% identity
478 resulted in 218 homologous groups (Supplemental file 1, Cluster3Uniref tab) that were assessed
479 with BLASTp for sequence level homology to experimentally characterized T11SS cargo
480 domains. Only a few sets of homologs were identified, even when including all TbpBBD-domain-
481 containing UniRef50 clusters. Homologs of six UniRef50 clusters, specific to the
482 *Rhodobacteraceae*/*Roseobacteriaceae* families, resembled the Hemophilin-like 1 architecture,
483 and homologs from another UniRef50 resembled the disordered N-terminus 1 architecture

484 noted previously (see Figs. 3 and 4). Collectively these 7 UniRef50 clusters encompass a total of
485 only 31 ORFs across 27 species/taxa (Supplemental file 1, Cluster3PutativeCargo tab). The ratio
486 of predicted cargo per T11SS OMP was far lower in cluster 3 (0.21 Cargo/input OMP) than it
487 was in cluster 1 (2.39 Cargo/input OMP). This dearth of co-occurring putative cargo proteins
488 suggests that marine cluster 3 T11SS OMPs seldom co-occur with their cognate cargo proteins,
489 utilize cargo proteins with below-threshold sequence similarity to those of cluster 1 T11SS, or
490 have evolved distinct functions and no longer have partner cargo proteins.

491 To further examine this potential transition in function, we comparatively annotated a
492 syntenic T11SS OMP-encoding locus in 11 representative *Rhodobacteraceae*/*Roseobacteriaceae*
493 strains (Supplemental file 3, Clus3SyntenicPairs tab). Each locus encodes all four of the top co-
494 occurring domains from our co-occurrence analysis, including flavin-dependent thymidylate
495 synthase, lactoylglutathione lyase, and one or more DUF1194 (Fig. 8A and Supplemental file 3,
496 NeighborhoodAlignment tab). All but one (*Pseudooceanicola marinus* LMG23705) of the loci
497 also encodes a protein that is predicted to be a T11SS cargo lipoprotein (282-375 aa) based on
498 the presence of an N-terminal SPII type signal sequence and a C-terminal 8-stranded β-barrel
499 domain (Fig. 5F; Fig. 8B-K) [21]. The presence of both cluster 1 and cluster 3 co-occurring
500 domains indicates that this conserved locus is a hybrid of the two. It is tempting to speculate
501 that this locus represents a transitional state in the divergence of these systems, with at least
502 one analyzed genome appearing to have lost the cluster 1 co-occurring, 8-stranded β-barrel
503 domain.

504 We next examined the cluster 3 marine T11SS co-occurrence dataset to consider the
505 possibility of alternative putative cargo types. In contrast to cluster 1 T11SS, co-occurrence with

506 TbpBBD/lipoprotein C domains, TonB-dependent receptors, and TonB domains are rare within
507 the marine cluster 3 T11SS loci. Instead, the DUF1194 domain (PF06707) was highly prevalent
508 (102/145 queries) (Supplemental file 4). Of the 102 DUF1194-containing sequences found in the
509 cluster 3 co-occurrence list, 7 are predicted to be lipoproteins, 76 are predicted to be soluble
510 Sec-secreted proteins, and 19 have no detectable signal peptide according to SignalP 6 [37, 38].
511 Many cluster 3 T11SS loci encoded 2 or 3 distinct DUF1194 genes in close proximity (e.g., Fig. 8),
512 predicted to encode both lipidated and non-lipidated proteins (e.g., algal symbiont
513 *Rhodobacteraceae* PD-2 ETA49263.2 and ETA49262.2, respectively) (Supplemental file 4). The
514 predicted RoseTTAFold structure [53] of the DUF1194 domain is a mixed β-strand/α-helix (Fig.
515 8). According to the Pfam database, the DUF1194 domain occurs in 31 distinct protein
516 architectures with other domains, including C-terminal autotransporter domain (PF03797)
517 predicted to function in T5SS secretion, the CARDB domain (PF07705), which adopts a 7 β-
518 strand structure, DUF11 (PF01345), predicted to have an 8-stranded β-barrel structure, and
519 PF18911, the known crystal structures of which also adopt a β-barrel (e.g., 1wgo and 2y72).

520 Of the co-occurring DUF1194 sequences, 6 are annotated as having homology to von
521 Willebrand factor type A domain or vWA (PF00092). This homology is reflected in the structural
522 similarity between these two domains, including the presence of a Rossman fold, which may
523 hint at similar molecular roles. vWA protein architectures can include divalent-cation-binding
524 metal ion-dependent adhesion sites (MIDAS), with a characteristic DxSxS…T…D motif [54, 55].
525 Almost all the DUF1194 proteins that co-occurred with DUF560 proteins contained at least one
526 MIDAS motif (98/102). To examine potential structural features of cluster 3 T11SS co-occurring
527 DUF1194-containing homologs, we focused on three adjacently encoded DUF1194 genes from

528 *Ascidiaceihabitans donghaensis* (SPH20589/SPH20588/SPH20587) for structural analysis.
529 PsiPred 4.0 predicted that these proteins have at least 5 predominantly hydrophobic β-strands,
530 all separated by α-helix regions in a structure that also appears to be a variation on the classical
531 α/β Rossman fold (Fig. 9A). RoseTTAFold predictions of the tertiary structure of these DUF1194
532 proteins reveal globular proteins wherein 6 hydrophobic β-strands form a β-sheet at the core of
533 the protein, which is protected by three α-helices per side. All three representatives had a
534 MIDAS motif starting 10-11 residues after the predicted signal peptide. For each protein, the
535 last 11-13 C-terminal residues appeared to be disordered, and their positions could not be
536 estimated with a high degree of confidence (Fig. 9B).

537 **Discussion**

538 The controlled bioinformatics analyses we report here reinforce the idea that cluster 1
539 T11SS-dependent cargo have roles in metal uptake, single carbon metabolism, and nutrient
540 provision. Further, our data extend the experimentally verified T11SS cargo to include
541 *Haemophilus parahaemolyticus* Pls and lend credence to the concept that T11SS cargo can be
542 bioinformatically predicted. The structural prediction that this cargo protein is a fusion between
543 a functional Pls domain, typical of Gram-positive bacteria, and a C-terminal 8-stranded β-barrel
544 domain lends further evidence of the function of the barrel domain in directing cargo to the
545 T11SS, and for the function of T11SS in facilitating transport across an outer membrane.
546 However, our analysis of the more distantly related cluster 3 T11SS OMPs revealed that known
547 barrel domains (TbpBBD and lipoprotein C) are rare among the significantly co-occurring genes
548 identified, raising the intriguing possibility that novel structural domains may exist that mediate
549 targeting to cluster 3 T11SS.

550 Our bioinformatic approach relied upon gene co-occurrence analysis, which uses
551 genomic proximity as a proxy for coordinate regulation and potential interactions, since genes
552 within a common functional pathway often cluster together within a genome. While this is not
553 a foolproof method , the use of large genomic datasets increases the power of co-occurrence
554 analysis to identify potential co-interacting partners [56]. One of the methodological
555 refinements we developed was the use of *in silico* controls for genome neighborhood co-
556 occurrence to reduce false positives and noise in the output datasets of putative T11SS co-
557 occurring protein families. For instance, activities associated with protein translation and RNA
558 metabolism, which are essential cellular processes expected to be present in every cell, are not
559 always useful co-occurrence signatures for elucidating T11SS function and components. Such
560 general functions are not indicative of the specific functions of T11SS relative to any other OMP
561 and can be considered a form of false negative, Type II error; such co-occurrences are not
562 biologically relevant, but are not being excluded from the analysis because they do co-occur
563 frequently with the query gene. However, removal of such co-occurrences can also lead to false
564 positive, Type I error, because they can also result in removal of some biologically relevant co-
565 occurrences. For example, there could be protein families that are important functional
566 partners of the query protein, but that are removed from the dataset if they were important for
567 both query and control proteins. This type of error occurred in our analysis. For example, TonB-
568 dependent receptors, with which many T11SS-dependent cargo interact, were excluded from
569 the cluster 1 T11SS analyses since these domains associate with other outer membrane
570 proteins unrelated to T11SS. In a sense, this control narrows the focus from total co-occurrence
571 to unique co-occurrence, and as such it is best suited towards applications in which the

572 researcher seeks to differentiate protein families. Additionally, the technique can be further
573 adapted and refined, depending on application. For instance, multiple non-specific gene
574 neighborhood controls could be generated by randomly subsampling the list of proteins that
575 are biophysically similar to the query proteins, allowing for increased stringency and measures
576 of variance.

577 The cluster 1 T11SS significantly co-occurring genes identified here are consistent with
578 previous observations [4, 7]. Iron uptake from the environment is a common function among
579 experimentally verified T11SS-dependent cargo proteins and this theme was extended within
580 the cluster 1 T11SS co-occurrence dataset, which included heme oxygenases and heme
581 transporters that facilitate iron uptake [57]. Similarly, the protein export genes identified as co-
582 occurring with cluster 1 T11SS included TonB and ExbD, which are essential to energize uptake
583 of nutrients from known T11SS-dependent cargo [8, 10, 58]. TolA is essential to bring
584 periplasmic nutrients into the cytoplasm of the cell [59]. Signal peptidase II is essential for the
585 generation of bacterial lipoproteins, which constitute a substantial percentage of T11SS-
586 dependent cargo [60]. Finally, the observed co-occurrence with transposases and tRNA-
587 synthases is consistent with the hypothesis that T11SS are regularly associated with mobile
588 genetic islands and can be horizontally acquired and contribute to fitness within a host
589 environment [36].

590 Significantly co-occurring pathways were commonly identified for both cluster 1 and
591 cluster 3 T11SS, and represent pathways not previously associated with T11SS. These included
592 folate (vitamin B9)-related pathways, including folate biosynthesis, folate-dependent enzymes,
593 and one carbon metabolism via folate. Folate, like heme, is an enzyme cofactor required for

594 many diverse biological pathways. It is essential for the function of thymidylate synthase
595 complementing protein, also known as flavin-dependent thymidylate synthase, in nucleotide
596 biosynthesis [61]. This protein is the third most common cluster 3 marine T11SS co-occurring
597 gene, suggesting coordinate regulation or inheritance. Since, unlike heme, folate does not
598 incorporate a metallic ion and most bacteria synthesize their folate instead of scavenging it
599 from the environment [62], we do not favor the hypothesis that folate itself is acquired through
600 a T11SS-dependent uptake mechanism. Instead, the close association of folate metabolism and
601 T11SS may reflect the fact that folate biosynthesis, as well as iron-sulfur cluster biosynthesis,
602 and methylotrophic metabolism by formate dehydrogenase (which also significantly co-
603 occurred with T11SS) depend on the metal-bearing enzyme cofactors, cobalamin (vitamin B12)
604 and molybdopterin cofactor (MoCo) [63–66]. Our data suggest that some T11SS OMPs may
605 function in cobalamin or molybdopterin uptake pathways. Regardless, our data clearly
606 demonstrate an association between T11SS and single carbon metabolism and methyltropism.

607 Cluster 1 T11SS co-occurrences featured TonB energization or heme/iron uptake that were
608 lacking from cluster 3 T11SS co-occurrences. In turn, the most frequent cluster 3 T11SS co-occurrences
609 were DUF1194 and lactoylglutathione lyase (GloA), neither of which appeared in the Cluster 1 T11SS co-
610 occurrence datasets, but both of which have connections to metal ions. The function of DUF1194 is
611 currently unknown but it is predicted to fold into a globular protein with an α/β Rossman fold.
612 Several of the DUF1194 proteins (6/103) we detected also had homology to a structurally
613 similar α/β Rossman fold domain called von Willebrand factor A (vWA), which is most often
614 associated with serum glycoproteins and large multimeric protein complexes in mammalian
615 systems [67, 68]. In *Myxococcus xanthus* bacteria, the vWA domain-containing surface

616 lipoprotein CglB acts as a surface adhesin essential for gliding motility [69]. Upon binding a
617 ligand, vWA domain-containing adhesins such as CglB can stabilize their bond via a
618 conformational change induced by MIDAS motif allosteric binding of a divalent metal cation,
619 often Mg^{2+}[55, 69]. The presence of a MIDAS motif in the vast majority of DUF1194 identified
620 within our dataset suggests that these proteins may also play a role in adhesion or may
621 participate in metal homeostasis in previously unpredicted ways. Additionally, vWA domain
622 containing proteins are involved in microbial conflict sensor systems called MoxR-vWA-centric
623 ternary systems, wherein a surface receptor protein receives an extracellular signal from a
624 symbiotic species and then signals a response using intracellular vWA chaperones and MoxR
625 ATPases [70, 71]. Although we did not detect MoxR homologs in our analysis, this example
626 raises the possibility that one role for T11SS OMPs may be to deliver sensor proteins to the cell
627 surface that relay signals to DUF1194 partners. Other possibilities, include that DUF1194
628 proteins themselves are a type of T11SS-dependent cargo, or that they contribute to a
629 multimeric protein complex that interacts with T11SS proteins. Lactoylglutathione lyase is an
630 enzyme with a coordinated metal ion (typically nickel) and functions in the regeneration step of
631 the glyoxalase-mediated aldehyde detoxification system [72]. It is possible that the nickel
632 requirement of this enzyme reflects a role for cluster 3 T11SS in facilitating nickel uptake.
633 Alternatively, this co-occurrence may indicate that cluster 3 T11SS are more generally
634 participating in an aldehyde producing process. Notably, aldehydes like methylglyoxal are
635 exceptionally cytotoxic and can damage DNA and proteins, so the cluster 3 T11SS co-occurrence
636 of nucleotide and amino acid biosynthesis may reflect a more general relationship between
637 T11SS and the aldehyde repair response [72, 73].

638 In addition to providing insights into functional pathways associated with T11SS, our
639 analysis also allowed us to identify 148 homology groups of putative T11SS-dependent cargo,
640 including those with domain architectures distinct from those found in known cargo. We
641 verified that at least one of these, the plasmin-sensitive surface protein (Pls) from the Gram-
642 negative organism *H. parahaemolyticus,* is a bona fide T11SS-dependent cargo protein,
643 demonstrating the efficacy of our bioinformatics approach. Pls represents a novel N-terminal
644 effector domain among T11SS cargo. This domain is homologous to glycosylated Pls proteins
645 found on or spontaneously cleaved from the surfaces of Gram-positive organisms such as
646 *Staphylococcus aureus* and *S. epidermidis* where function in biofilm formation and modulating
647 adhesion to host proteins [44, 45]. Given that the function of Pls requires surface exposure, its
648 presence in a Gram-negative organism is complicated by the existence of the outer membrane.
649 In *H. parahaemolyticus*, this hurdle seems to have been overcome via fusion of the Pls repeat
650 domain to the C-terminal 8-stranded β-barrel domain necessary for cluster 1 T11SS-dependent
651 secretion across the outer membrane [4, 7].

652 When co-expressed in *E. coli* with its T11SS partner, TepS*,* Pls predominantly localizes to
653 the supernatant and is not tethered to the cell surface as would be expected of a lipoprotein.
654 Our working model is that some Pls can reach the cell surface in the absence of T11SS, as has
655 been observed for factor H binding protein [74, 75], and that in the presence of the T11SS TepS,
656 Pls is secreted but then cleaved, releasing it into the extracellular milieu. Given that our
657 experiments were conducted in a protease-deficient strain of *E. coli*, it will be exciting in future
658 studies to determine if TepS alters the topology of Pls in order to make it susceptible to
659 proteolysis, or if it is directly responsible for Pls cleavage, which would be a novel function for

660 T11SS. The possibility that Gram-negative Pls are secreted via T11SS and may be released from
661 the cell surface in the process will be an important factor to consider in ongoing efforts to
662 target Pls homologs for vaccine development, such as that being pursued for *Actinobacillus*
663 *pleuropneumoniae* Pls (YP_001652736.1) [76]. Also, the Pls-like proteins have repeat rich
664 regions and the possible glycosylation of *H. parahaemolyticus* Pls is supported by our
665 observations of its aberrant mobility in SDS-PAGE. It is possible that other T11SS-dependent
666 cargo, including lipoproteins, may also be glycosylated. If so, such glycoproteins tethered to the
667 cell surface would display glycans as surface antigens that may modulate host-microbe
668 recognition and immune evasion [77–79].

669 In summary, our findings have enhanced our understanding of potential effectors of the
670 novel T11SS and expanded the list of experimentally verified T11SS secreted cargo. We also
671 have expanded the field of genomic co-occurrence analysis by establishing a protocol that can
672 serve as a basis for more controlled and specific experimental designs. Exciting avenues of
673 future research could focus on generating an automated pipeline for controlling co-occurrences
674 analyses, determining if Pls is required for host-colonization by *Haemophilus parahaemolyticus*,
675 investigating if DUF1194 represents a novel T11SS cargo type, and exploring the relationship
676 between one carbon metabolism and T11SS.

677

678 **Conflicts of interest**

679 The author(s) declare that there are no conflicts of interest.

680

681 **Funding information**

682 This work was funded, in part, by funds awarded to H.G.-B. from the University of Tennessee-
683 Knoxville (David and Sandra White Endowment) and the National Science Foundation (IOS-
684 2128266).

685

686 **Author contributions**

687 ASG: Conceptualization, data curation, formal analysis, investigation, methodology, validation,
688 writing original draft and review/editing

689 NCM: Conceptualization, data curation, investigation, formal analysis, methodology, writing
690 original draft

691 SJK: Investigation, methodology

692 JR: Investigation

693 HGB: Conceptualization, data curation, funding acquisition, investigation, methodology, project
694 administration, resources, supervision, visualization, writing original draft and review/editing

695

696 **Acknowledgements**

697 We thank past and present members of the Goodrich-Blair lab for feedback on the
698 development of controls for bioinformatic co-occurrence analyses.

699 **References:**

700 1. **Grossman AS, Mucci NC, Kauffman SJ, Rafi J, Goodrich-Blair H**. Bioinformatic discovery of type
701 11 secretion system (T11SS) cargo across the Proteobacteria supplemental data. *Figshare. Online*
702 *resource*. Epub ahead of print 5 March 2025. DOI: 10.6084/m9.figshare.28514069.v2.

703 2. **Mistry J, Chuguransky S, Williams L, Qureshi M, Salazar G, *et al.*** Pfam: The protein families
704 database in 2021. *Nucleic Acids Res* 2021;49:D412–D419.

705 3. **Mudgal R, Sandhya S, Chandra N, Srinivasan N**. De-DUFing the DUFs: Deciphering distant
706 evolutionary relationships of domains of unknown function using sensitive homology detection
707 methods. *Biol Direct* 2015;10:38.

708 4. **Grossman AS, Mauer TJ, Forest KT, Goodrich-Blair H, Comstock L**. A widespread bacterial
709 secretion system with diverse substrates. *mBio* 2022;12:e01956-21.

710 5. **Huynh MS, Hooda Y, Li YR, Jagielnicki M, Lai CC-L, *et al.*** Reconstitution of surface lipoprotein
711 translocation through the Slam translocon. *Elife*;11. Epub ahead of print April 2022. DOI:
712 10.7554/eLife.72822.

713 6. **Shin HE, Pan C, Curran DM, Bateman TJ, Chong DHY, *et al.*** Prevalence of Slam-dependent
714 hemophilins in Gram-negative bacteria. *J Bacteriol* 2024;206:e00027-24.

715 7. **Hooda Y, Lai CC-L, Moraes TF**. Identification of a large family of Slam-dependent surface
716 lipoproteins in Gram-negative bacteria. *Front Cell Infect Microbiol*;7. Epub ahead of print 2017.
717 DOI: 10.3389/fcimb.2017.00207.

718 8. **Hooda Y, Lai CC-L, Judd A, Buckwalter CM, Shin HE, *et al.*** Slam is an outer membrane protein
719 that is required for the surface display of lipidated virulence factors in *Neisseria*. *Nat Microbiol*;1.
720 Epub ahead of print 2016. DOI: 10.1038/nmicrobiol.2016.9.

721 9. **Cowles CE, Goodrich-Blair H**. The *Xenorhabdus nematophila* nilABC genes confer the ability of
722 *Xenorhabdus* spp. to colonize *Steinernema carpocapsae* nematodes. *J Bacteriol* 2008;190:4121–
723 4128.

724 10. **Bateman TJ, Shah M, Ho TP, Shin HE, Pan C, *et al.*** A Slam-dependent hemophore contributes to
725 heme acquisition in the bacterial pathogen *Acinetobacter baumannii*. *Nat Commun*
726 2021;12:6270.

727 11. **Latham RD, Torrado M, Atto B, Walshe JL, Wilson RK, *et al.*** A heme-binding protein produced by
728 *Haemophilus haemolyticus* inhibits non-typeable *Haemophilus influenzae*. *Mol Microbiol*
729 2020;113:381–398.

730 12. **Grossman AS, Gell DA, Wu DG, Carper DL, Hettich RL, *et al.*** Bacterial hemophilin homologs and
731 their specific type eleven secretor proteins have conserved roles in heme capture and are
732 diversifying as a family. *J Bacteriol* 2024;206:e00444-23.

733 13. **Sam F, Brianna A, Arianna M, J HK, S RJ, *et al.*** Heme sequestration by hemophilin from
734 *Haemophilus haemolyticus* reduces respiratory tract colonization and infection with non-
735 typeable *Haemophilus influenzae*. *mSphere* 2024;9:e00006-24.

736 14. **Haft DH, Badretdin A, Coulouris G, DiCuccio M, Durkin AS, *et al.*** RefSeq and the prokaryotic
737 genome annotation pipeline in the age of metagenomes. *Nucleic Acids Res* 2024;52:D762–D769.

738 15. **Rogozin IB, Makarova KS, Murvai J, Czabarka E, Wolf YI, *et al.*** Connected gene neighborhoods in
739 prokaryotic genomes. *Nucleic Acids Res* 2002;30:2212–2223.

740 16. **Mahdavi MA, Lin Y-H**. False positive reduction in protein-protein interaction predictions using
741 gene ontology annotations. *BMC Bioinformatics* 2007;8:262.

742 17. **Tietz JI, Schwalen CJ, Patel PS, Maxson T, Blair PM, *et al.*** A new genome-mining tool redefines
743 the lasso peptide biosynthetic landscape. *Nat Chem Biol* 2017;13:470–478.

744 18. **The UniProt Consortium**. UniProt: The universal protein knowledge base in 2021. *Nucleic Acids*
745 *Res* 2021;49:D480–D489.

746 19. **Chen I-MA, Chu K, Palaniappan K, Ratner A, Huang J, *et al.*** The IMG/M data management and
747 analysis system v.7: content updates and new features. *Nucleic Acids Res* 2023;51:D723–D732.

748 20. **Mukherjee S, Stamatis D, Li CT, Ovchinnikova G, Bertsch J, *et al.*** Twenty-five years of Genomes
749 OnLine Database (GOLD): data updates and new features in v.9. *Nucleic Acids Res* 2023;51:D957–
750 D963.

751 21. **Jumper J, Evans R, Pritzel A, Green T, Figurnov M, *et al.*** Highly accurate protein structure
752 prediction with AlphaFold. *Nature* 2021;596:583–589.

753 22. **Mirdita M, Schütze K, Moriwaki Y, Heo L, Ovchinnikov S, *et al.*** ColabFold: Making protein folding
754 accessible to all. *Nat Methods* 2022;19:679–682.

755 23. **Abramson J, Adler J, Dunger J, Evans R, Green T, *et al.*** Accurate structure prediction of
756 biomolecular interactions with AlphaFold 3. *Nature* 2024;630:493–500.

757 24. **Aramaki T, Blanc-Mathieu R, Endo H, Ohkubo K, Kanehisa M, *et al.*** KofamKOALA: KEGG
758 Ortholog assignment based on profile HMM and adaptive score threshold. *Bioinformatics*
759 2020;36:2251–2252.

760 25. **Kanehisa M, Sato Y, Morishima K**. BlastKOALA and GhostKOALA: KEGG tools for functional
761 characterization of genome and metagenome sequences. *J Mol Biol* 2016;428:726–731.

762 26. **Suzek BE, Huang H, McGarvey P, Mazumder R, Wu CH**. UniRef: comprehensive and non-
763 redundant UniProt reference clusters. *Bioinformatics* 2007;23:1282–1288.

764 27. **Buchan DWA, Jones DT**. The PSIPRED protein analysis workbench: 20 years on. *Nucleic Acids Res*
765 2019;47:W402–W407.

766 28. **Bhasin A, Chaston JM, Goodrich-Blair H**. Mutational analyses reveal overall topology and
767 functional regions of NilB, a bacterial outer membrane protein required for host association in a
768 model of animal-microbe mutualism. *J Bacteriol* 2012;194:1763–1776.

769 29. **Miroux B, Walker JE**. Over-production of proteins in *Escherichia coli*: mutant hosts that allow
770 synthesis of some membrane proteins and globular proteins at high levels. *J Mol Biol*
771 1996;260:289–298.

772 30. **Dumon-Seignovert L, Cariot G, Vuillard L**. The toxicity of recombinant proteins in *Escherichia coli*:
773 a comparison of overexpression in BL21(DE3), C41(DE3), and C43(DE3). *Protein Expr Purif*
774 2004;37:203–206.

775 31. **Orchard SS, Goodrich-Blair H**. Identification and functional characterization of a *Xenorhabdus*
776 *nematophila* oligopeptide permease. *Appl Environ Microbiol* 2004;70:5621–5627.

777 32. **Grossman AS, Escobar CA, Mans EJ, Mucci NC, Mauer TJ, *et al.*** A surface exposed, two-domain
778 lipoprotein cargo of a type XI secretion system promotes colonization of host intestinal epithelia
779 expressing glycans. *Frontiers in Microbiology*;13.
780 https://www.frontiersin.org/article/10.3389/fmicb.2022.800366 (2022).

781 33. **Koontz L**. Chapter one - TCA precipitation. In: Lorsch JBT-M in E (editor). *Laboratory methods in*
782 *enzymology*. Academic Press. pp. 3–10.

783 34. **Tukey JW**. Comparing individual means in the analysis of variance. *Biometrics* 1949;5:99–114.

784 35. **Kanehisa M, Furumichi M, Tanabe M, Sato Y, Morishima K**. KEGG: New perspectives on
785 genomes, pathways, diseases and drugs. *Nucleic Acids Res* 2017;45:D353–D361.

786 36. **Dobrindt U, Reidl J**. Pathogenicity islands and phage conversion: Evolutionary aspects of bacterial
787 pathogenesis. *International Journal of Medical Microbiology* 2000;290:519–527.

788 37. **Almagro Armenteros JJ, Tsirigos KD, Sønderby CK, Petersen TN, Winther O, *et al.*** SignalP 5.0
789 improves signal peptide predictions using deep neural networks. *Nat Biotechnol* 2019;37:420–
790 423.

791 38. **Teufel F, Almagro Armenteros JJ, Johansen AR, Gíslason MH, Pihl SI, *et al.*** SignalP 6.0 predicts
792 all five types of signal peptides using protein language models. *Nat Biotechnol* 2022;40:1023–
793 1025.

794 39. **Skaf MS, Polikarpov I, Stanković IM**. A linker of the proline-threonine repeating motif sequence
795 is bimodal. *J Mol Model* 2020;26:178.

796 40. **Swearingen KE, Lindner SE, Shi L, Shears MJ, Harupa A, *et al.*** Interrogating the *Plasmodium*
797 sporozoite surface: identification of surface-exposed proteins and demonstration of glycosylation
798 on CSP and TRAP by mass spectrometry-based proteomics. *PLoS Pathog* 2016;12:e1005606.

799 41. **Sieber CMK, Paul BG, Castelle CJ, Hu P, Tringe SG, *et al.*** Unusual metabolism and hypervariation
800 in the genome of a Gracilibacterium (BD1-5) from an oil-degrading community. *mBio*;10. Epub
801 ahead of print November 2019. DOI: 10.1128/mBio.02128-19.

802 42. **Calmettes C, Alcantara J, Yu R-H, Schryvers AB, Moraes TF**. The structural basis of transferrin
803 sequestration by transferrin-binding protein B. *Nat Struct Mol Biol* 2012;19:358–360.

804 43. **Ostberg K, DeRocco A, Mistry S, Dickinson Mary K, Cornelissen CN**. Conserved regions of
805 gonococcal TbpB are critical for surface exposure and transferrin iron utilization. *Infect Immun*
806 2013;81:3442–3450.

807 44. **Bleiziffer I, Eikmeier J, Pohlentz G, McAulay K, Xia G, *et al.*** The Plasmin-sensitive protein Pls in
808 methicillin-resistant *Staphylococcus aureus* (MRSA) is a glycoprotein. *PLoS Pathog*
809 2017;13:e1006110.

810 45. **Savolainen K, Paulin L, Westerlund-Wikström B, Foster TJ, Korhonen TK, *et al.*** Expression of *pls*,
811 a gene closely associated with the *mecA* gene of methicillin-resistant *Staphylococcus aureus*,
812 prevents bacterial adhesion *in vitro*. *Infect Immun* 2001;69:3013–3020.

813 46. **Liang KYH, Orata FD, Boucher YF, Case RJ**. Roseobacters in a sea of poly- and paraphyly: Whole
814 genome-based taxonomy of the family Rhodobacteraceae and the proposal for the split of the
815 "Roseobacter Clade" into a novel family, Roseobacteraceae fam. nov. *Front Microbiol*;12. Epub
816 ahead of print 2021. DOI: 10.3389/fmicb.2021.683109.

817 47. **Crenn K, Serpin D, Lepleux C, Overmann J, Jeanthon C**. *Silicimonas algicola* gen. nov., sp. nov., a
818 member of the Roseobacter clade isolated from the cell surface of the marine diatom
819 *Thalassiosira delicatula*. *Int J Syst Evol Microbiol* 2016;66:4580–4588.

820 48. **Kessner L, Spinard E, Gomez-Chiarri M, Rowley DC, Nelson DR**. Draft genome sequence of
821 *Aliiroseovarius crassostreae* CV919-312, the causative agent of Roseovarius Oyster Disease
822 (formerly Juvenile Oyster Disease). *Genome Announc*;4. Epub ahead of print March 2016. DOI:
823 10.1128/genomeA.00148-16.

824 49. **Kim Y-O, Park S, Nam B-H, Lee C, Park J-M, *et al.*** *Ascidiaceihabitans donghaensis* gen. nov., sp.
825 nov., isolated from the golden sea squirt *Halocynthia aurantium*. *Int J Syst Evol Microbiol*
826 2014;64:3970–3975.

827 50. **Ivanova EP, Gorshkova NM, Sawabe T, Zhukova N V, Hayashi K, *et al.*** *Sulfitobacter delicatus* sp.
828 nov. and *Sulfitobacter dubius* sp. nov., respectively from a starfish (*Stellaster equestris*) and sea
829 grass (*Zostera marina*). *Int J Syst Evol Microbiol* 2004;54:475–480.

830 51. **Chen M-H, Sheu S-Y, Chen CA, Wang J-T, Chen W-M**. *Roseivivax isoporae* sp. nov., isolated from
831 a reef-building coral, and emended description of the genus *Roseivivax*. *Int J Syst Evol Microbiol*
832 2012;62:1259–1264.

833 52. **Alamos P, Tello M, Bustamante P, Gutiérrez F, Shmaryahu A, *et al.*** Functionality of tRNAs
834 encoded in a mobile genetic element from an acidophilic bacterium. *RNA Biol* 2018;15:518–527.

835 53. **Baek M, DiMaio F, Anishchenko I, Dauparas J, Ovchinnikov S, *et al.*** Accurate prediction of
836 protein structures and interactions using a three-track neural network. *Science (1979)*
837 2021;373:871–876.

838 54. **Bergelson JM, Hemler ME**. Integrin- Ligand Binding: Do integrins use a 'MIDAS touch' to grasp an
839 Asp? *Current Biology* 1995;5:615–617.

840 55. **Cantí C, Nieto-Rostro M, Foucault I, Heblich F, Wratten J, *et al.*** The metal-ion-dependent
841 adhesion site in the Von Willebrand factor-A domain of alpha2delta subunits is key to trafficking
842 voltage-gated Ca2+ channels. *Proc Natl Acad Sci U S A* 2005;102:11230–11235.

843 56. **Esch R, Merkl R**. Conserved genomic neighborhood is a strong but no perfect indicator for a
844 direct interaction of microbial gene products. *BMC Bioinformatics* 2020;21:5.

845 57. **Hantke K**. Is the bacterial ferrous iron transporter FeoB a living fossil? *Trends Microbiol*
846 2003;11:192–195.

847 58. **Ollis AA, Postle K**. ExbD mutants define initial stages in TonB energization. *J Mol Biol*
848 2012;415:237–247.

849 59. **Levengood SK, Beyer WFJ, Webster RE**. TolA: a membrane protein involved in colicin uptake
850 contains an extended helical region. *Proc Natl Acad Sci U S A* 1991;88:5939–5943.

851 60. **Tjalsma H, Kontinen VP, Prágai Z, Wu H, Meima R, *et al.*** The role of lipoprotein processing by
852 signal peptidase II in the Gram-positive eubacterium *Bacillus subtilis*. Signal peptidase II is
853 required for the efficient secretion of alpha-amylase, a non-lipoprotein. *J Biol Chem*
854 1999;274:1698–1707.

855 61. **Agrawal N, Lesley SA, Kuhn P, Kohen A**. Mechanistic studies of a flavin-dependent thymidylate
856 synthase. *Biochemistry* 2004;43:10295–10301.

857 62. **Dawadi S, Kordus SL, Baughn AD, Aldrich CC**. Synthesis and analysis of bacterial folate
858 metabolism intermediates and antifolates. *Org Lett* 2017;19:5220–5223.

859 63. **Luk LYP, Javier Ruiz-Pernía J, Dawson WM, Roca M, Loveridge EJ, *et al.*** Unraveling the role of
860 protein dynamics in dihydrofolate reductase catalysis. *Proc Natl Acad Sci U S A* 2013;110:16344–
861 16349.

862 64. **Mendel RR**. The molybdenum cofactor. *J Biol Chem* 2013;288:13165–13172.

863 65. **Zhong Q, Kobe B, Kappler U**. Molybdenum enzymes and how they support virulence in
864 pathogenic bacteria. *Frontiers in Microbiology*;11.
865 https://www.frontiersin.org/articles/10.3389/fmicb.2020.615860 (2020).

866 66. **Van Bibber M, Bradbeer C, Clark N, Roth JR**. A new class of cobalamin transport mutants (*btuF*)
867 provides genetic evidence for a periplasmic binding protein in *Salmonella typhimurium*. *J*
868 *Bacteriol* 1999;181:5539–5541.

869 67. **Peyvandi F, Garagiola I, Baronciani L**. Role of von Willebrand factor in the haemostasis. *Blood*
870 *Transfus* 2011;9 Suppl 2:s3-8.

871 68. **Von Willebrand EA**. Hereditary pseudohaemophilia. *Haemophilia* 1999;5:223–31; discussion 222.

872 69. **Islam ST, Jolivet NY, Cuzin C, Belgrave AM, My L, *et al.*** Unmasking of the von Willebrand A-
873 domain surface adhesin CglB at bacterial focal adhesions mediates myxobacterial gliding motility.
874 *Sci Adv* 2023;9:eabq0619.

875 70. **Aravind L, Iyer LM, Burroughs AM**. Discovering biological conflict systems through genome
876 analysis: Evolutionary principles and biochemical novelty. *Annu Rev Biomed Data Sci* 2022;5:367–
877 391.

878 71. **Kaur G, Burroughs AM, Iyer LM, Aravind L**. Highly regulated, diversifying NTP-dependent
879 biological conflict systems with implications for the emergence of multicellularity. *Elife*
880 2020;9:e52696.

881 72. **Lee C, Park C**. Bacterial responses to glyoxal and methylglyoxal: Reactive electrophilic species. *Int*
882 *J Mol Sci*;18. Epub ahead of print January 2017. DOI: 10.3390/ijms18010169.

883 73. **Anaya-Sanchez A, Feng Y, Berude JC, Portnoy DA**. Detoxification of methylglyoxal by the
884 glyoxalase system is required for glutathione availability and virulence activation in *Listeria*
885 *monocytogenes*. *PLoS Pathog* 2021;17:e1009819.

886 74. **Fantappiè L, Irene C, De Santis M, Armini A, Gagliardi A, *et al.*** Some Gram-negative lipoproteins
887 keep their surface topology when transplanted from one species to another and deliver foreign
888 polypeptides to the bacterial surface. *Molecular & Cellular Proteomics* 2017;16:1348 LP – 1364.

889 75. **Konar M, Rossi R, Walter H, Pajon R, Beernink PT**. A mutant library approach to identify
890 improved meningococcal Factor H binding protein vaccine antigens. *PLoS One* 2015;10:e0128185.

891 76. **Cao Y, Gao L, Zhang L, Zhou L, Yang J, *et al.*** Genome-wide screening of lipoproteins in
892 *Actinobacillus pleuropneumoniae* identifies three antigens that confer protection against virulent
893 challenge. *Sci Rep* 2020;10:2343.

894 77. **Schmidt MA, Riley LW, Benz I**. Sweet new world: Glycoproteins in bacterial pathogens. *Trends*
895 *Microbiol* 2003;11:554–561.

896 78. **Tortorelli G, Rautengarten C, Bacic A, Segal G, Ebert B, *et al.*** Cell surface carbohydrates of
897 symbiotic dinoflagellates and their role in the establishment of cnidarian-dinoflagellate
898 symbiosis. *ISME J* 2022;16:190–199.

899 79. **Zhou M, Wu H**. Glycosylation and biogenesis of a family of serine-rich bacterial adhesins.
900 *Microbiology (N Y)* 2009;155:317–327.

901
902

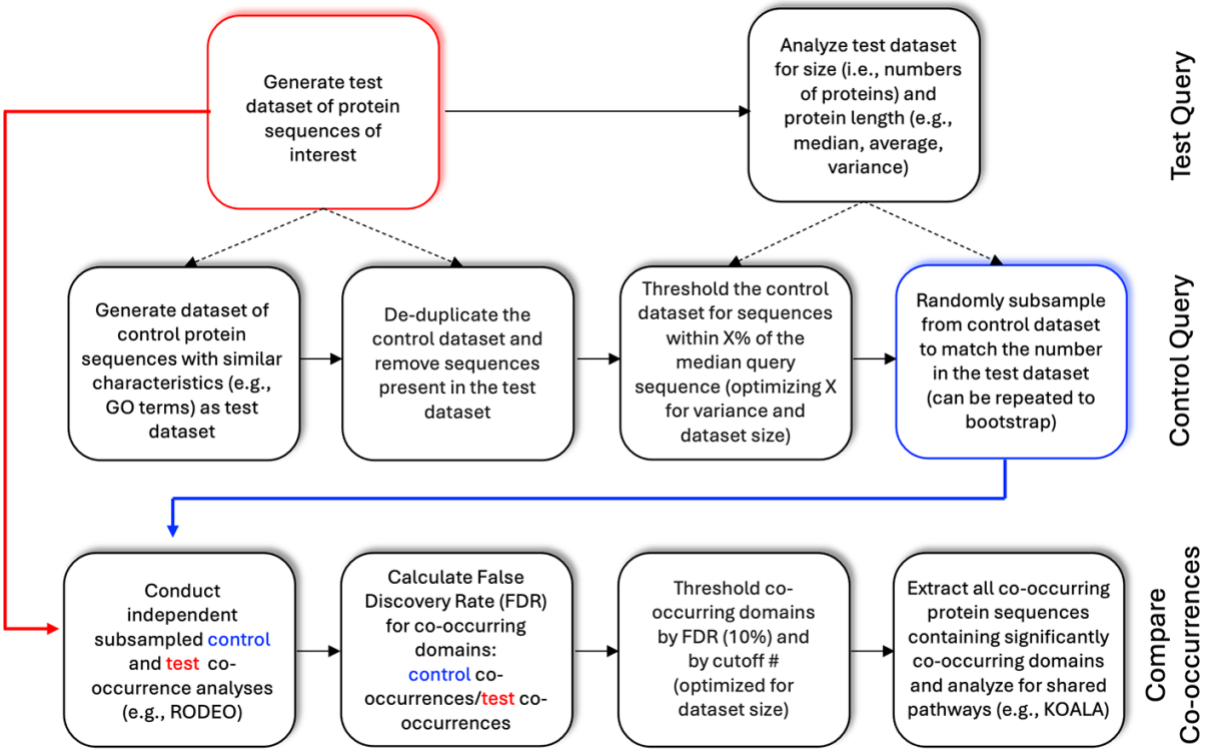

Figure 1. **Design for a novel control technique for genomic neighborhood co-occurrence analysis.** Logic flowchart to control for nonspecific co-occurrences from a genomic neighborhood analysis. For the analyses presented here, the test dataset queries comprised two different clusters (1 and 3) of T11SS OMPs identified in a published network analysis [4]. Control datasets were developed for each cluster separately. The thresholds for the control datasets were set with X% determined as how many +/- amino acids resulted in the # of proteins that was close to, yet over, each test dataset.

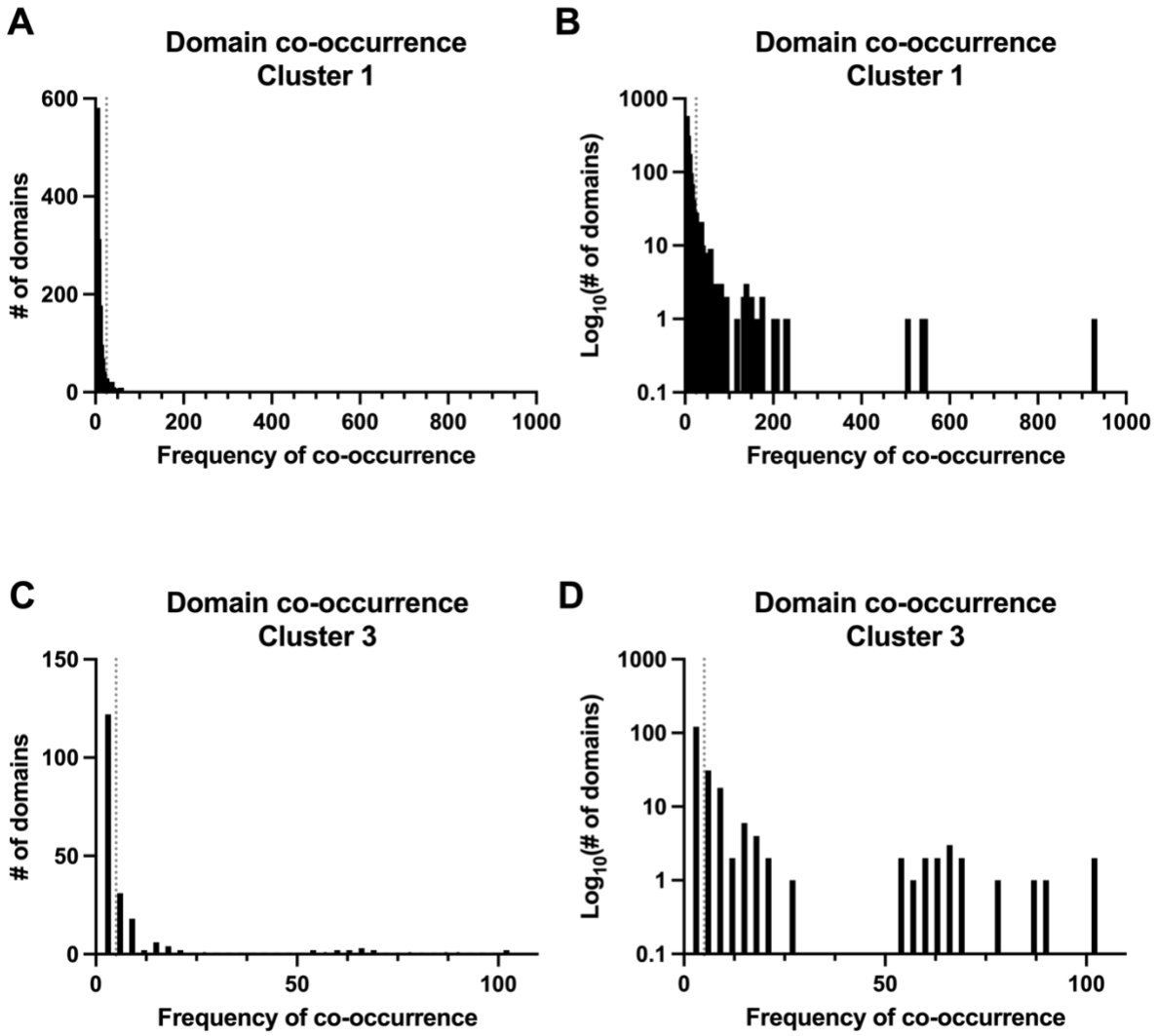

Supplemental Figure 1. **Histograms displaying the distribution of co-occurrence frequency amongst domains co-occurring with T11SS.** Genomic neighborhood analysis detects many domains within assayed loci (6 open reading frames up- and down-stream of each T11SS), however the majority of domains only co-occur a small number of times. To filter out rare or spurious co-occurrences, a threshold of co-occurrence is established relative to the size of your dataset. Histograms depict the frequency of domain co-occurrence with animal-associated cluster 1 T11SS **(A)** and with marine-associated cluster 3 T11SS **(C)**. Log_{10} transformation of these values **(B, D)** helps to visualize domains with many co-occurrences. The dotted lines on all graphs show the thresholds chosen for filtering each dataset.

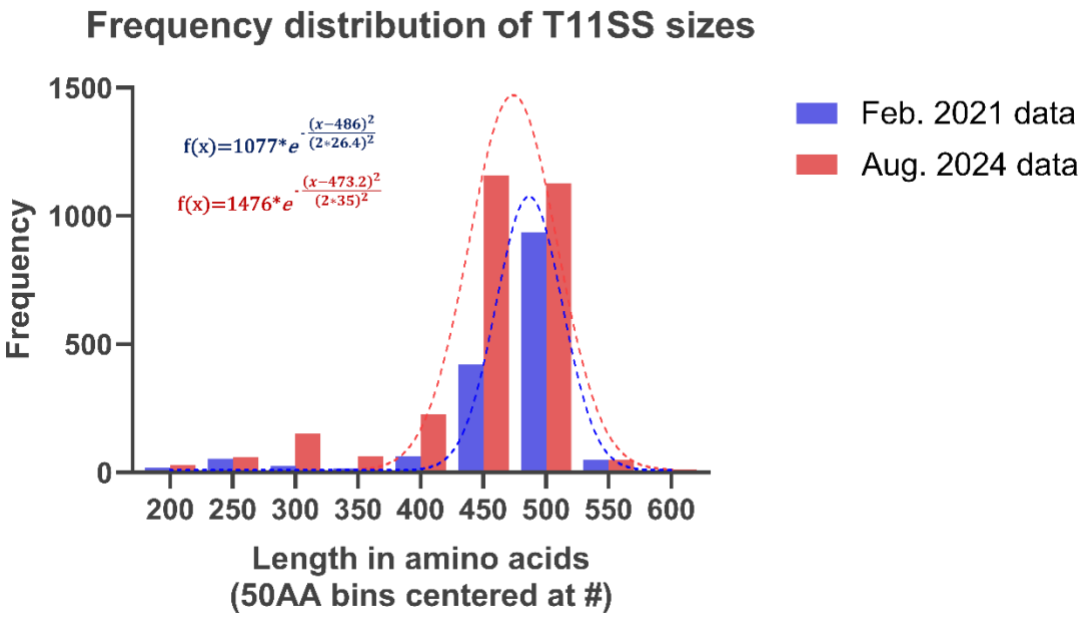

925

926 Supplemental Figure 2. **T11SS (DUF560) protein size distribution (in amino acids).** After
927 examination of the size distribution, median was chosen as an appropriate measure of
928 representative protein size over mean due to left-skewed distribution. The blue dataset was
929 used to perform the T11SS co-occurrence analysis described in this manuscript. In the
930 intervening time more homologs have been added to the Pfam database, the red dataset
931 reflects these additions and their impact on the size distribution.
932

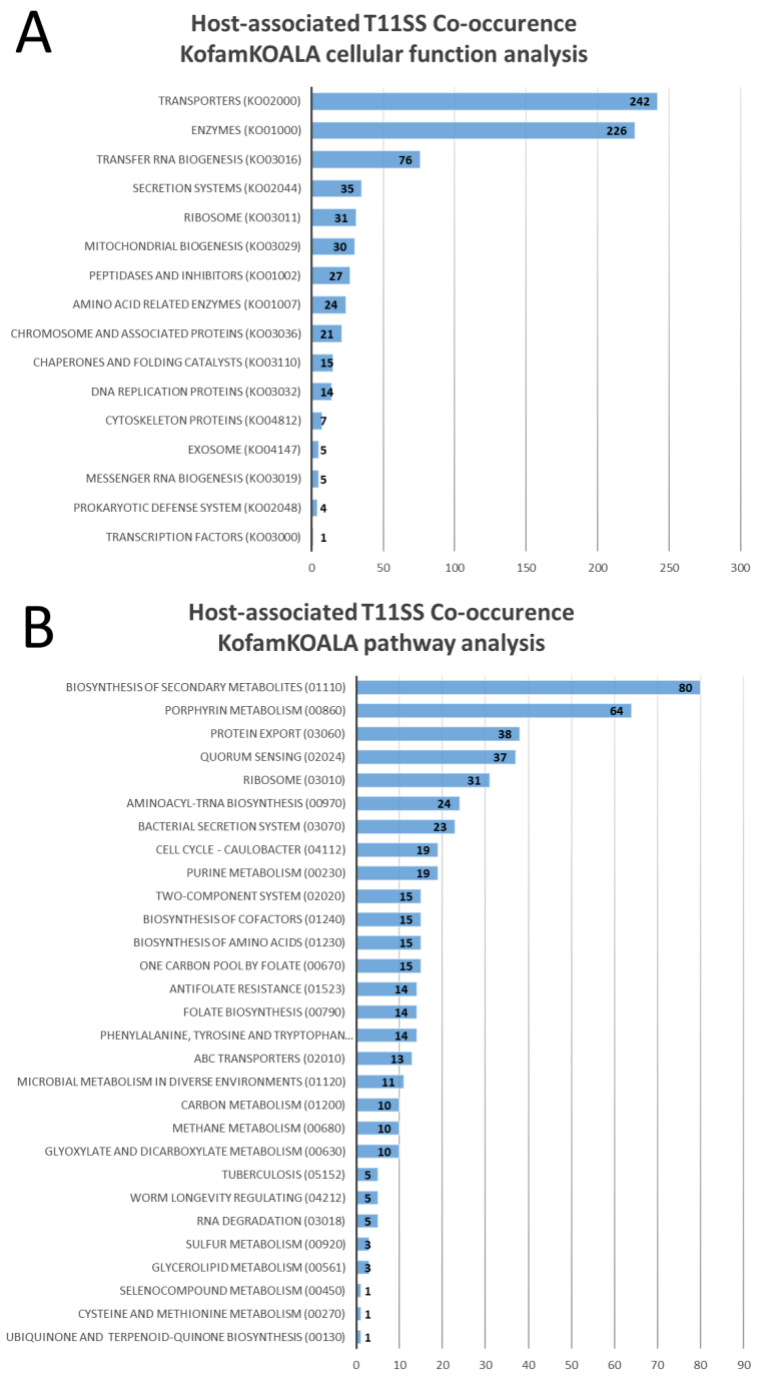

Figure 2. **Host-associated T11SS genome neighborhoods reveal conserved association with iron/heme uptake, export, and one-carbon metabolism**. KofamKOALA uses hidden Markov models to assign functions to query sequences and reveal shared pathways. Cellular functions **(A)** were estimated using BRITE hierarchies and, where possible, assigned to known pathways **(B)** to detect commonalities.

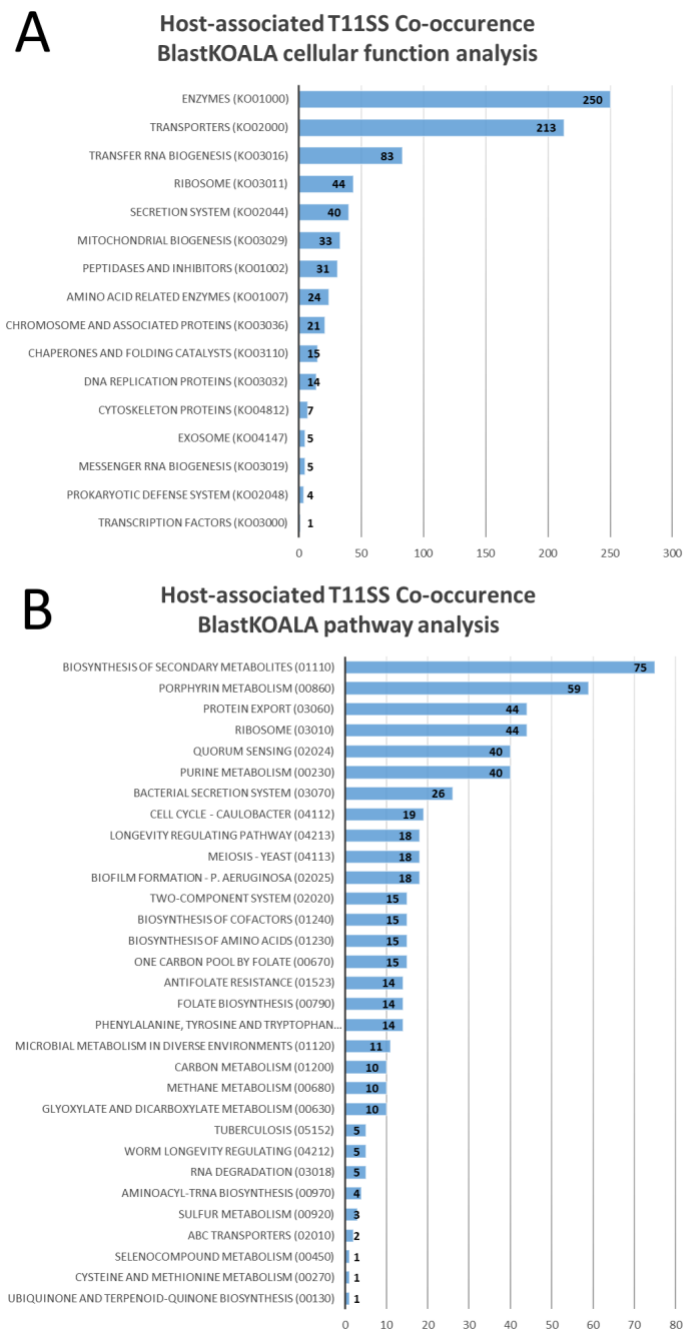

Supplemental Figure 3. **BlastKOALA supports T11SS association with iron/heme uptake, protein export, and one-carbon metabolism**. BlastKOALA uses the BLAST alignment algorithm to assign functions to query sequences and reveal shared pathways. Cellular functions **(A)** were estimated using BRITE hierarchies and assigned, where possible, to known pathways **(B)** to detect commonalities.

Figure 3. **Secondary structure of predicted T11SS-dependent cargo reveals diverse and novel gene architectures and effector domains**. PsiPred 4 and DisoPred 3 use amino acid sequence to annotate secondary structures highlighting a diversity of N-terminal domains with proline rich repeats, intrinsically disordered regions, α-helical repeats, and ligand binding handles. For each of the detected cargo architectures the representative sequence from the largest UniRef50 cluster was trimmed of it signal peptide to reflect a mature protein.

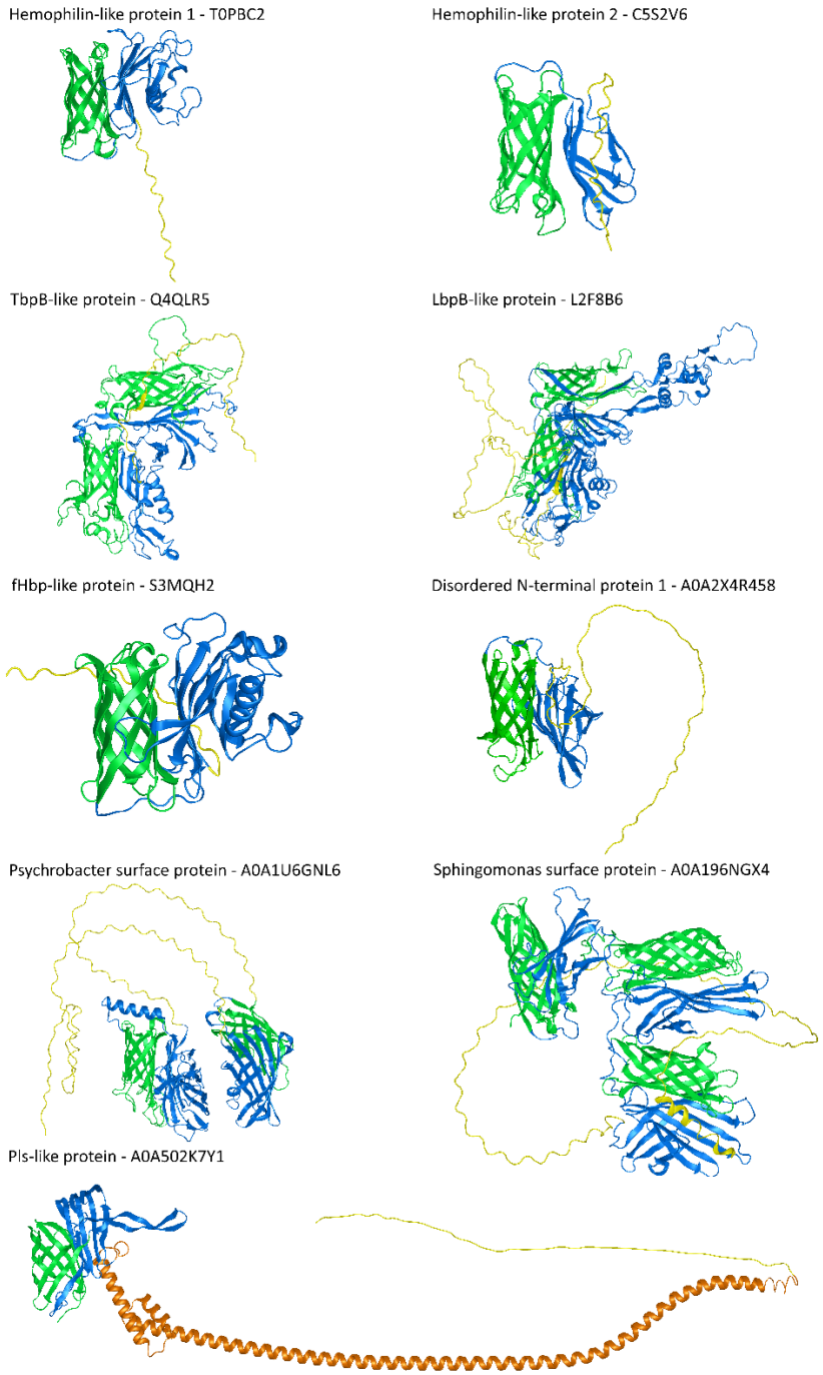

952

953 Figure 4. **AlphaFold2 annotation of predicted T11SS-dependent cargo reveals conservation of**
954 **C-terminal or centrally located β-barrel domains**. For each of the detected cargo architectures
955 the representative sequence from the largest UniRef50 cluster was used to predict a
956 representative structure. Green residues indicate C-terminal β-barrel domains. Blue residues
957 indicate putative ligand binding handle domains. Orange residues indicate glycosylation motif

958 repeats within the Pls-like protein architecture. Yellow residues indicate regions predicted to be
959 disordered.

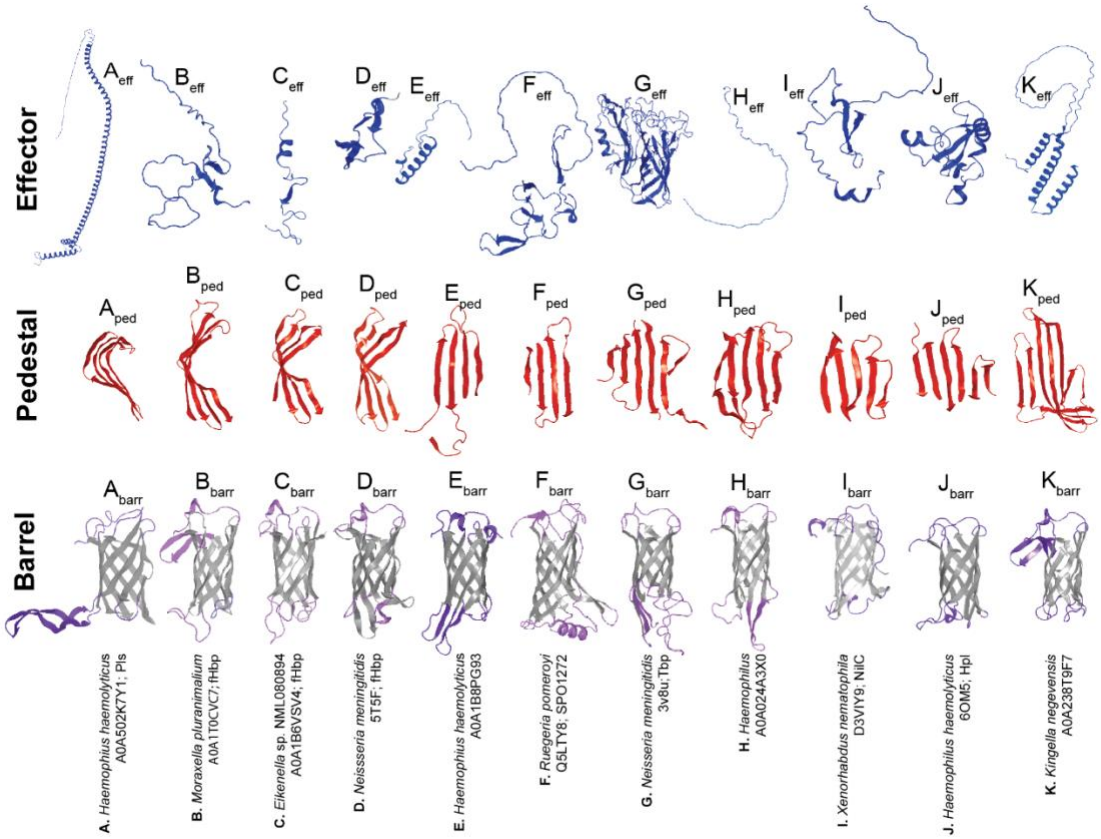

Figure 5. **AlphaFold2 annotation of predicted T11SS-dependent cargo reveals three distinct domains ubiquitous to cargo.** Solved **(D, G, J)** or predicted **(A, B, C, E, F, H, I, K)** structures from representative UniRefF50 cluster sequences of predicted **(A, B, D, E, F, H, K)** or known cargo **(D, G, I, J)**. Each structure was separated into three sections representing common structural domains: N-terminal effector (blue), pedestal (red), and C-terminal β-barrel (gray barrel residues and purple loop residues). N-terminal effector domains varied in their predicted structural motifs and included disordered **(B, C, D, H, I)**, α-helical **(A, E, K)**, β-strand **(D, F, J)**, and barrel **(G)**. Pedestal domains comprised 4-stranded groove **(A)**, 4-stranded "wing" **(B-D),** 4-stranded sheet **(E, F)**, 5-stranded sheet **(G-I)**, or 6-stranded/extended β-sheet **(J, K)**. Some of these β-strands are donated by primary sequences from either the N-terminus or the C-terminus of the protein. Barrel domains exhibited variation in the presence of extended loops, helices, or strands in predicted surface- or periplasmic-exposed regions, as indicated by purple coloration.

974

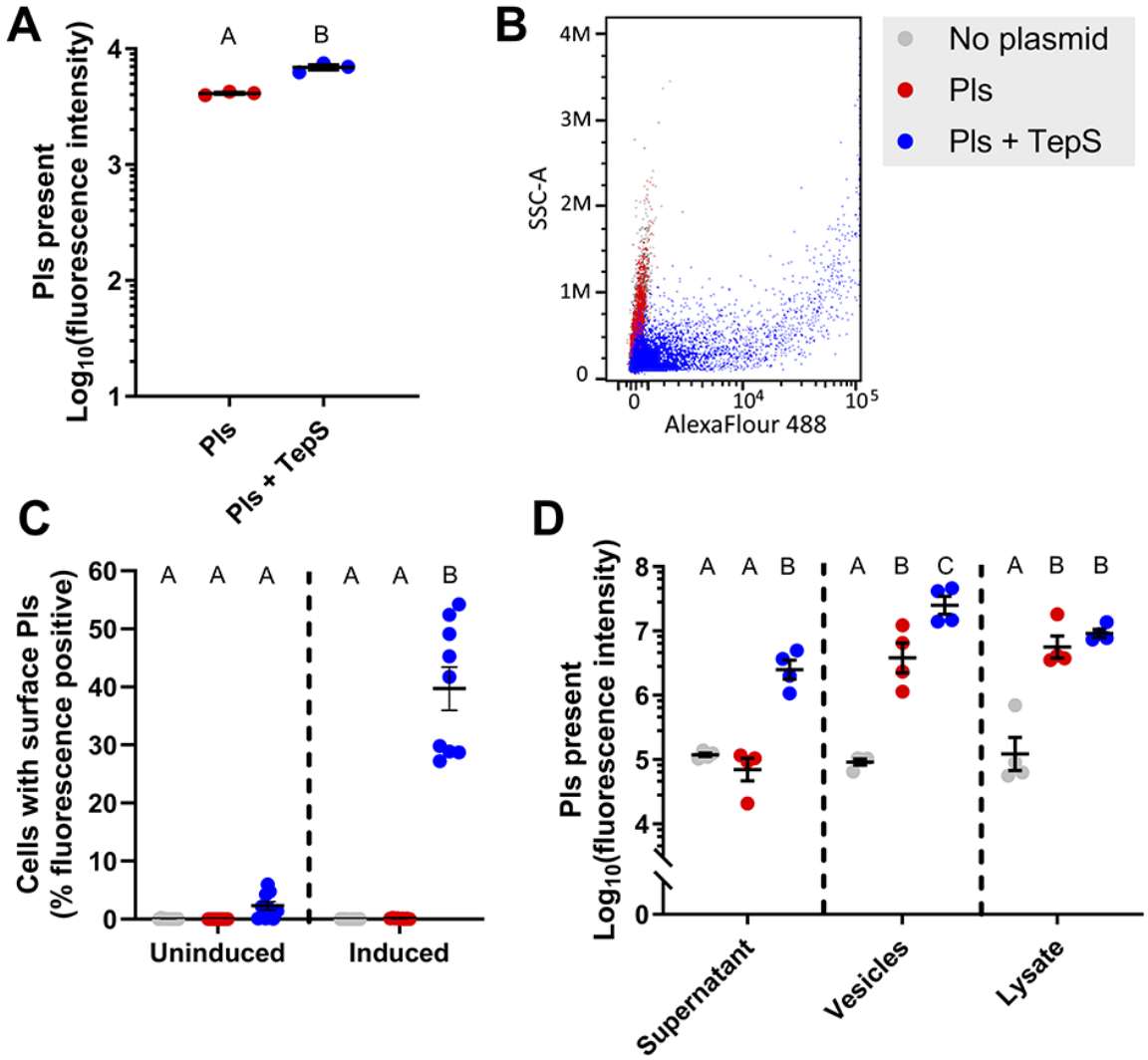

975

976 Figure 6. **Localization of FLAG tagged Pls in the absence and presence of its cognate T11SS**
977 **secretor.** *E. coli* cells expressing Pls-FLAG alone or Pls-FLAG alongside its cognate T11SS (TepS)
978 were probed using Western blotting (lysates from flow cytometry samples, supernatants, and
979 extracellular vesicles), flow cytometry (cell surface exposure), and immuno-dot blots (lysates
980 from supernatant collections) to see how expression of the T11SS protein impacted protein
981 localization. Strong expression of Pls was detected in lysates from both strains **(A and D)**. A
982 representative flow cytometry replicate **(B)** shows that surface exposed Pls was only detectable
983 on cells co-expressing TepS **(C)**. For each biological replicate 100,000 events were detected via
984 flow cytometry. Supernatant secretion of Pls was also only detectable in the presence of TepS
985 **(D)**. The extracellular vesicle fraction collected via ultracentrifugation showed some Pls
986 localization in the absence of TepS, however that localization was significantly increased by
987 TepS. One-way ANOVA with Tukey's HSD statistical test used to compare treatments in all

988 experiments, letters above treatments indicate significance groups at p value 0.05. Error bars
989 indicate standard error of the mean.

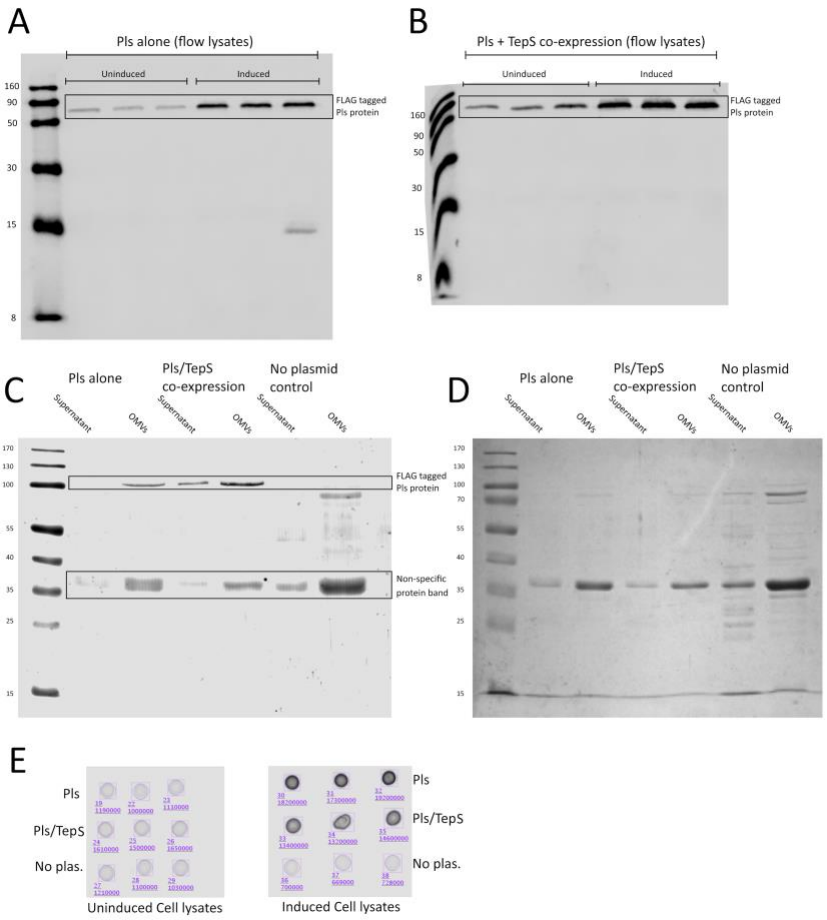

Supplemental Figure 4. **Localization of FLAG tagged Pls in the absence and presence of its cognate T11SS secretor.** Samples from *E. coli* cells expressing Pls-FLAG alone or Pls-FLAG and its cognate T11SS (TepS) were probed with α-FLAG antibody using Western blotting (lysates from flow cytometry samples, supernatants, and extracellular vesicles) **(panels A-C)** or dot blots (lysates from supernatant collections) **(panel E)** to determine if expression of the T11SS-protein TepS impacted Pls protein localization. Representative Western blots demonstrating comparable levels of Pls expression in flow cytometry cultures in Pls only **(A)** and Pls and TepS **(B)** expressing cells. **(C)** A representative Western blot showing α-FLAG-antibody reactive supernatant proteins separated into soluble and vesicle fractions. **(D)** A representative Coomassie stain showing total supernatant protein content separated into soluble and vesicle fractions. **(E)** Immuno-dot blots demonstrating comparable levels of Pls expression in lysates from supernatant collection cultures.

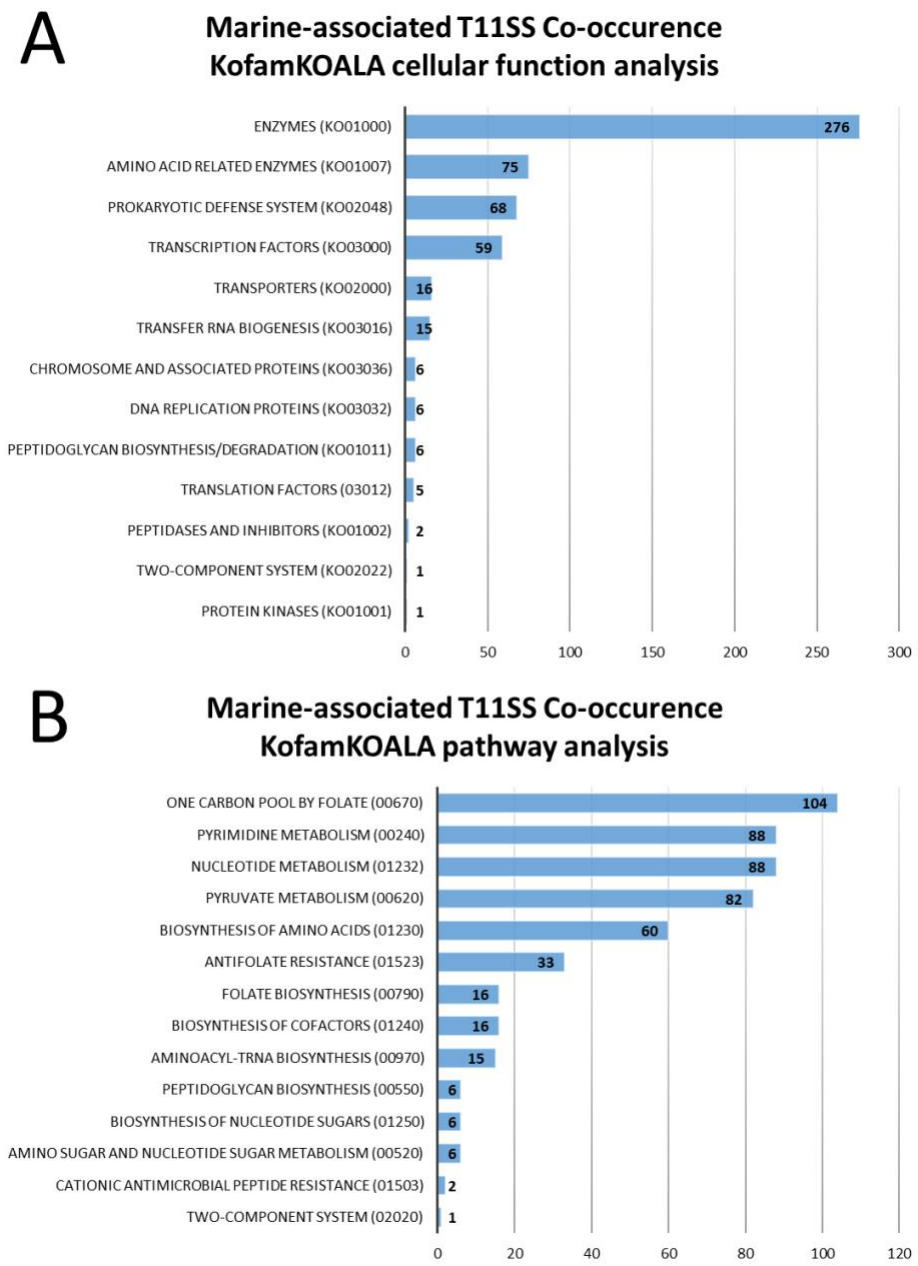

Figure 7. **Marine T11SS genome neighborhoods reveal association with one-carbon metabolism, nucleotide metabolism, and the glyoxalase-detoxification pathway**. KofamKOALA uses hidden Markov models to assign functions to query sequences and reveal shared pathways. Cellular functions **(A)** were estimated using BRITE hierarchies and assigned, where possible, to known pathways**(B)**.

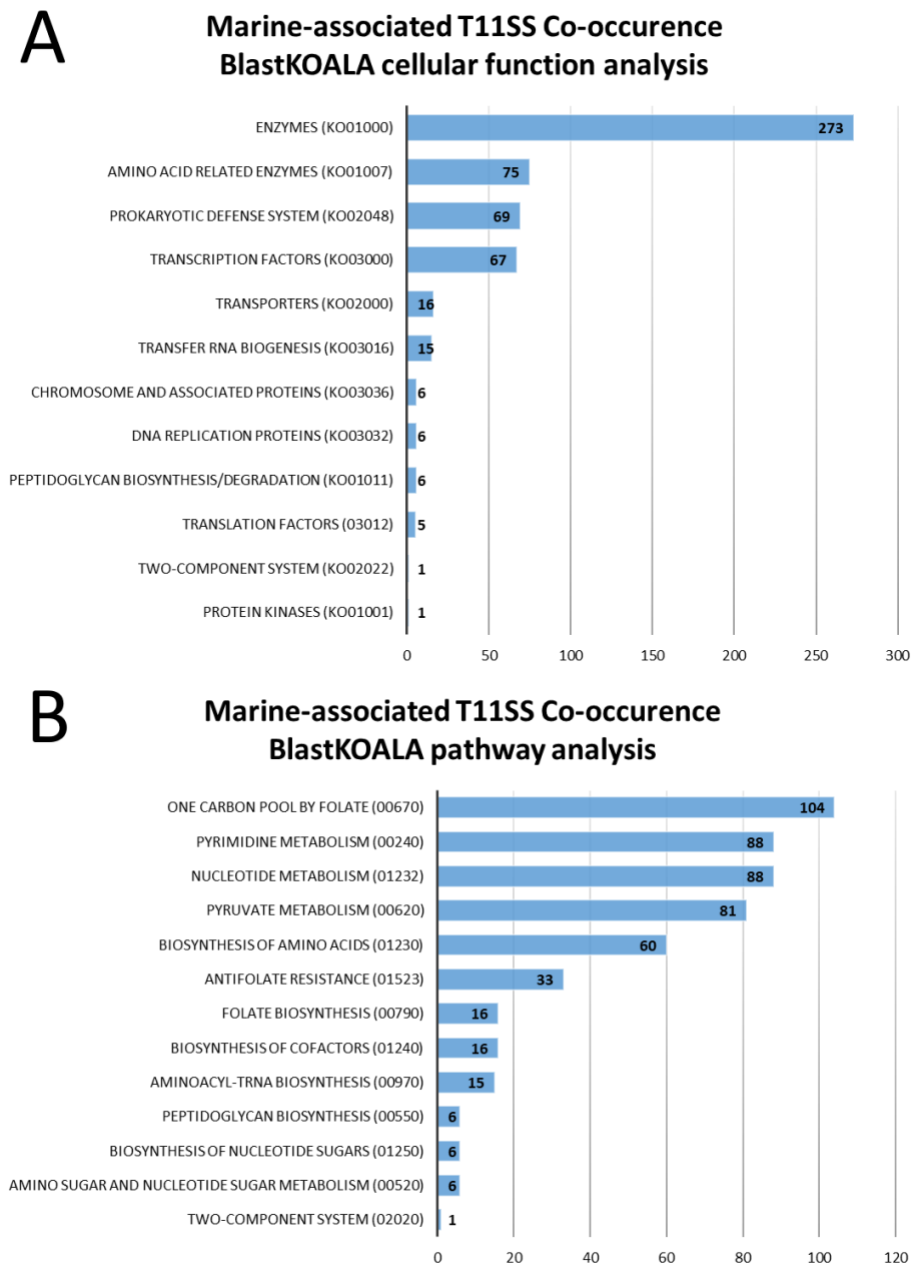

Supplemental Figure 5. **BlastKOALA supports T11SS association with one-carbon metabolism, nucleotide metabolism, and the glyoxalase-detoxification pathway**. BlastKOALA uses the BLAST alignment algorithm to assign functions to query sequences and reveal shared pathways. Cellular functions **(A)** were estimated using BRITE hierarchies and assigned, where possible, to known pathways **(B)**.

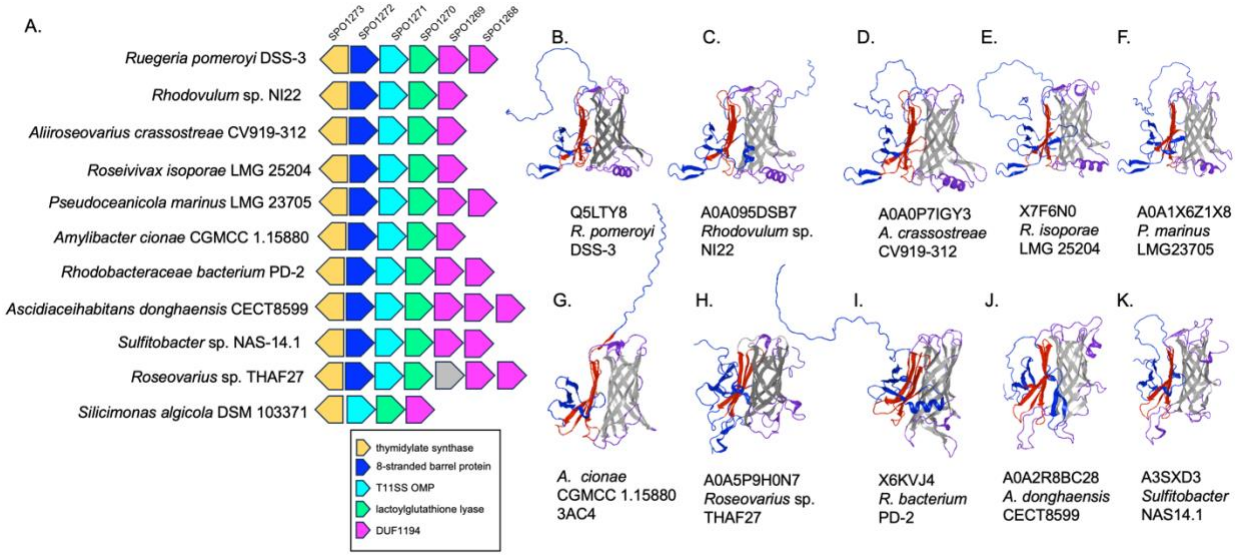

Figure 8. **A conserved marine cluster 3, T11SS OMP locus encodes predicted cargo proteins.** A schematic representation of select examples of a T11SS OMP-encoding, syntenic locus found with genomes of indicated strains of *Rhodobacteraceae* and *Roseobacteriaceae* **(A)**. Each gene is represented by a block arrow (not to scale), and the *Ruegeria pomeroyi* locus tags of each homolog are indicated at the top. In all 11 genomes examined, the syntenic locus included genes predicted to encode a T11SS OMP (turquoise arrows) as well as the top cluster 3 co-occurring functions: flavin-dependent thymidylate synthase (gold arrows), lactoylglutathione lyase (neon green arrows), and one or more DUF1194/von Willebrand factor proteins (pink arrows). In all but one, the locus includes a putative T11SS cargo protein (light blue arrows), identified based on the presence of a predicted C-terminal 8-stranded β-barrel domain. Predicted AlphaFold 2.0 or AlphaFold 3.0 predicted structures of putative cargo proteins encoded within these loci is shown in **(B-K)**. Color coding is used to indicate the putative effector (dark blue), pedestal (red), barrel (gray), and surface or periplasmic loops (purple) of each protein. The top five appear to have similar structural motifs, including an α-helix in one of the β-barrel loops, antiparallel β-strands in the N-terminal domain (blue), and a 4-stranded sheet pedestal domain (red). The remaining five structures show the overall domains of N-terminal (blue), pedestal (red) and β-barrel (gray), but the N-terminal domains are predicted to have different structural motifs relative to the others examined.

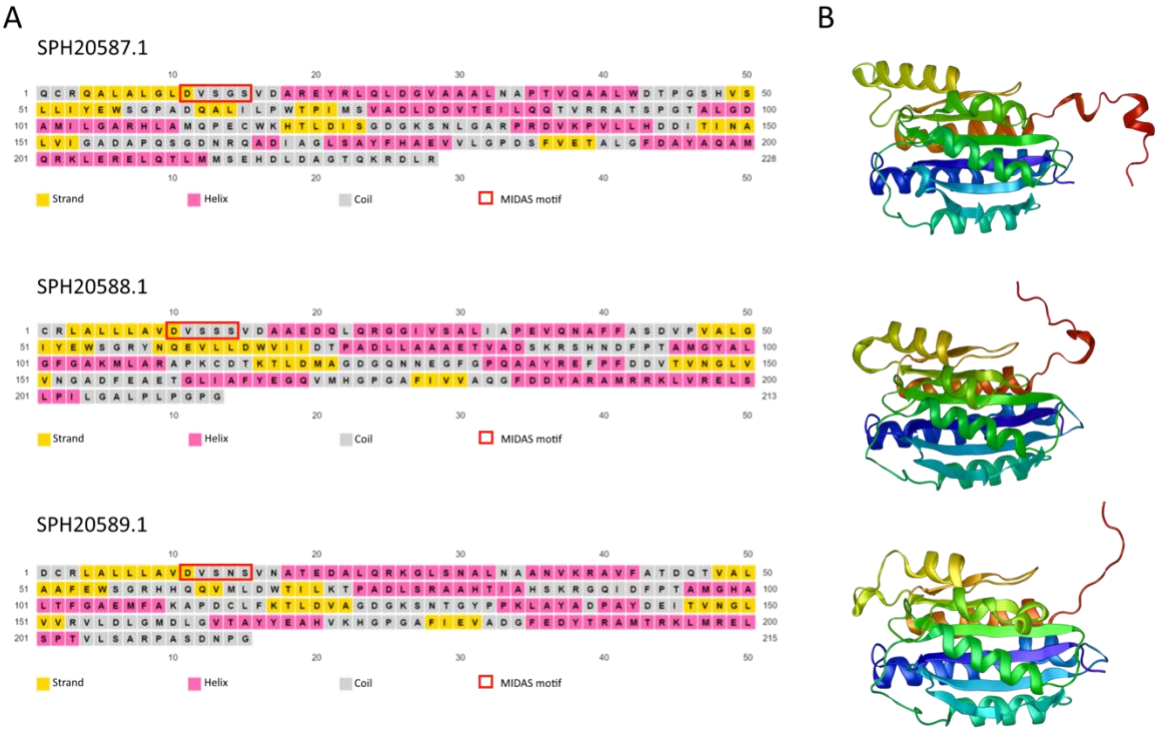

Figure 9. **Representative structures of DUF1194 proteins located within a T11SS genomic neighborhood in *Ascidiaceihabitans donghaensis***. These three DUF1194 homologs are encoded adjacent to a T11SS OMP-encoding gene within a microbe isolated from a tunicate host. These proteins appear to be paralogs of each other based on sequence similarity. Signal peptides were predicted with SignalP 6 and trimmed from the sequences prior to submission to PsiPred **(A)** and RoseTTAFold **(B).**

1044 Supplemental Files:

1045 Supplemental File 1: **T11SSGenomicCo-occurrence.xlsx**
1046 Controlled co-occurrence analysis of all domains and genes significantly co-occurring with
1047 T11SS in a cluster of host-associated organisms (cluster 1) or a cluster of marine organisms
1048 (cluster 3). Significant genes were then clustered into UniRef50 clusters to combine close
1049 homologs and mined for predicted T11SS cargo proteins via homology to known cargo proteins.
1050
1051 Supplemental File 2: **Co-occurrenceFunctionalAnnotations.xlsx**
1052 KEGG based analysis genes significantly co-occurring with host associated T11SS (cluster 1) and
1053 a marine T11SS (cluster 3).
1054
1055 Supplemental File 3: **Cluster3CargoLoci.xlsx**
1056 Selected Cluster 3 predicted cargo proteins co-occurring with T11SS.
1057
1058 Supplemental File 4: **T11SS-DUF1194Co-occurrence.xlsx**
1059 Co-occurrence of Marine associated T11SS alongside DUF1194 domain encoding genes, color
1060 coded to indicate host-associated organisms.